Title: An assessment of ERT as a method to monitor water content regime in flood embankments: the case study of the Adige River embankment.

Authors: Alessia Amabile[a], Bruna de Carvalho Faria Lima Lopes[a], Annarita Pozzato[a], Vojtech Benes[b], Alessandro Tarantino[a]

a. University of Strathclyde, Glasgow, UK

Address: Civil and Environmental Engineering Department,

75 Montrose Street - Glasgow G1 1XJ, Scotland, UK

b. G Impuls Praha Ltd.

Address: Přístavní 531/24, 170 00 Praha 7-

Holešovice, Czech Republic

Corresponding author: Alessia Amabile

E-mail: alessia.amabile@strath.ac.uk

Abstract

Stability of flood embankments is strongly affected by the water flow taking place in the saturated and unsaturated soil. Monitoring of the water flow in flood embankments is therefore essential in the context of flood risk management to predict and prevent failures of embankments. Electrical Resistivity Tomography (ERT) is gaining popularity for its ability to monitor water regime in the subsoil more quickly, cost-effectively and on a larger scale compared to traditional geotechnical monitoring systems that rely on local sensors. This paper presents the application of ERT to the monitoring of water content in a flood embankment on the Adige River in Italy. The resistivity profiles obtained from the ERT measurements were converted into water content profiles via a laboratory-derived relationship between resistivity and water content. At the same time, local sensors to monitor pore water pressure were installed in the saturated and unsaturated zone of the embankment and this allowed reconstructing the water content regime in the embankment via inverse analysis of water flow. This offered the chance to benchmark ERT-derived water content against independent indirect measurements of water content in the field.

ERT-inferred water content profiles based on laboratory calibration could capture the water content profiles derived from water flow analysis only qualitatively. This was attributed to artefacts in the ERT data inversion arising from the high contrasts in resistivity between different embankment layers. On the other hand, ERT proved to be a valuable tool to quantify the water content in the soil if field-specific relationship between water content and ERT-measured resistivity is developed.

Keywords: Electrical Resistivity Tomography; Water content monitoring; Flood embankment; Time Domain Reflectometry

1 Introduction

River embankments are often used as a defence measures to protect people and properties against floods. When the river level changes water flows through the embankment and alters the pore water pressure distribution, and consequently the shear strength of the soil. This may lead to instability of the embankment and its failure to protect the floodplain. Characterisation of water flow is therefore very important to assess the stability of flood embankment and understand their failure mechanisms. Water flow often develops through preferential flow paths in the embankments because of the heterogeneity and spatial variability of soils. Preferential flow paths cannot be captured by traditional geotechnical monitoring systems, which are based on local sensors like piezometers. Geophysical methods are indirect methods that allow estimating water content, among other parameters, based on the physical properties of the sub-surface materials (Reynolds, 2011). Geophysical methods offer an attractive and valuable tool to carry out diffuse monitoring of water regime in geotechnical structures such as flood embankments. Geophysical methods are non-intrusive, cost-effective and can be employed to monitor water regime at a larger scale compared to local sensors.

Electrical Resistivity Tomography (ERT) is a common geophysical investigation technique. It is based on the measurement of apparent resistivity when an electric field is generated by injecting current in the subsoil by means of electrodes. The apparent resistivity measurements are then converted into a model of subsurface resistivity distribution of the soil through a process of forward modelling and inversion (Loke & Barker, 1995).

ERT is widely used for geological and hydrogeological surveys (Aning, et al., 2013) (Ramachandran, et al., 2012). Routine applications include contaminant detection (Ntarlagiannis, et al., 2016) and site investigations (Banham & Pringle, 2011), but it is also applied for subsurface investigations in different fields like archaeology (Leucci & Greco, 2012).

Electrical resistivity in unsaturated soils is strongly dependent on the moisture content, among other variables such as grain size and temperature (Samouelian, et al., 2005). Resistivity profiles offer a qualitative assessment of water content in the subsoil, with lower resistivity associated to higher moisture content and higher resistivity associated to low moisture content. For this reason ERT is a versatile tool and has found applications in the monitoring of seepage in earth structures (Johansson & Dahlin, 1996) (Lin, et al., 2013).

The relationship between water content and resistivity for a specific soil is described by generalised Archie's law (Archie, 1942). If the calibration parameters of Archie's law can be derived experimentally, either via laboratory testing or in the field, variations in resistivity can be used to quantify variations in moisture content and map water content in the subsoil.

This has found a variety of applications in the monitoring of water regime in the subsoil, from the interaction between soil and vegetation (Fan, et al., 2015) to the detection of permafrost (Hilbich, et al., 2009). Due to the importance of water flow in slope stability problems, ERT has also been used for landslide monitoring at different locations (Lebourg, et al., 2010); (Gance, et al., 2016). It has also found applications in the monitoring of water content in earth structures such as railway embankments (Chambers, et al., 2014) or highway embankments (Gunn, et al., 2015) (Glendinning, et al., 2014). This technique has been acknowledged as a valuable tool for monitoring water flow in flood prone areas (Brunet, et al., 2010) and it has recently found applications in the monitoring of water content in flood embankments. It can be conveniently implemented to investigate seasonal variations of water regime as a permanent monitoring system by burying the electrodes in the soil and transferring the data remotely, to correlate water content variation to weather events and parameters (Tresoldi, et al., 2019); (Jodry, et al., 2019).

Interpretation of ERT results can be complicated and affected by uncertainties for several reasons, including anomalies in the resistivity due to improper contact between electrodes and ground surface (Jodry, et al., 2019), numerical artefacts generated during the inversion process and effects of three-dimensional structures in the survey areas which cannot be accounted for in a two-dimensional model (Hojat, et al., 2020). Moreover the resistivity values are influenced by other variables (e.g. temperature) and there may be inaccuracies in the calibration parameters of Archie's law. It is therefore essential to validate water content values derived from ERT data against independent direct or indirect measurements of water content.

In this paper the soil electrical resistivity data derived from ERT measurements are used to map water content profiles in a flood embankment located on the Adige River in the North of Italy. The soil specific relationship between soil resistivity and water content was derived experimentally in the laboratory using Time Domain Reflectometry (TDR) on intact and compacted samples collected from the embankment. A geotechnical monitoring system consisting of piezometers and tensiometers was installed to measure pore water pressure above and below the water table respectively in the same location where ERT measurements were carried out. This offered the chance to benchmark ERT-derived water content profiles against the water content derived from numerical simulations based on the inverse analysis of the piezometer and tensiometer data.

2 The case study

The study site is located along the Adige River, in the North of Italy, near the village of San Floriano. The soil profile was characterised from borehole logs and DPH tests carried out on a 500 m segment from chainage km 122.000 to km 122.500 (Amabile, et al., 2020). The geophysical investigation focused on the area between chainage km 122.410 and km 122.460. The soil profile of a representative cross section of this segment is shown in Fig. 1. This area was chosen because a monitoring system consisting of tensiometers and piezometers is installed in the same segment (Amabile, et al., 2020), thus offering the chance to compare water content estimated from resistivity measurements to water content based on inverse analysis of the monitoring data.

Two materials can be identified in the embankment. The shell surrounding the core of the embankment and the berm built on the landside are made of coarse gravel and sand, shown by the shaded area in Fig. 1, while the core of the embankment is a brown sandy silt of fluvial origin and has a thickness of about 5 m. The foundation material is a coarse sand of fluvial origin corresponding to the ancient riverbed of the Adige River (Amabile, et al., 2020).

Intact samples were collected from the embankment core in a Shelby tube in order to characterise experimentally the relationship between resistivity and water content via laboratory testing. Additional samples were collected at different depths for the geotechnical characterisation of the material (Fig. 1). The grain size distribution for the material in the embankment core was obtained from two loose samples taken at a depth of 3.3 m and is shown in Fig. 2.

3 Laboratory determination of the relationship between resistivity and water content

3.1 Electrical resistivity measurements with TDR

3.1.1 Theoretical background

Time Domain Reflectometry (TDR) is a technique to measure the time-domain envelopes of electromagnetic waves propagating through waveguides installed into the soil. It can be used to measure the soil electrical conductivity via the measurement of the standing wave ratio.

The TDR system consists of a step pulse generator which generates electromagnetic waves and an oscilloscope which records voltage variations. Electromagnetic waves are transmitted through a probe connected to the oscilloscope and pulse generator via a coaxial cable (Tarantino, et al., 2008). Multiple reflections and transmissions of the electromagnetic wave take place at the head and at the end of the probe, until a stable level (standing wave) is achieved.

TDR systems often return the signal recorded by the oscilloscope in terms of reflection coefficient *R*:

$$R(t) = \frac{V(t) - V_0}{V_0} \qquad \textbf{Eq. 1}$$

where V is the reflected voltage and V_0 is the incident voltage, i.e. the voltage going into the head of the probe.

Topp et al. (1988) have shown that the bulk electrical conductivity of a soil can be measured by using TDR and applying the Giese & Tiemann (1975) equation:

$$\sigma = \frac{1}{Z_c}\frac{\varepsilon_o c Z_p}{L}\left[\frac{1 - R_\infty}{1 + R_\infty}\right] \qquad \textbf{Eq. 2}$$

where ε_0 is the permittivity of free space ($8.854 \cdot 10^{-12}$ F m^{-1}), c is the speed of light ($3 \cdot 10^8$ m s^{-1}), L is the probe span (m) , R_∞ the final (standing wave) reflection coefficient returned by the oscilloscope, Z_c is the impedance of the cable tester (Ω), and Z_p is the impedance of the probe (Ω).

By introducing the probe constant K_p

$$K_p = \frac{\varepsilon_o c Z_p}{L} \qquad \textbf{Eq. 3}$$

Eq. 2 can be rewritten as follows:

$$\sigma = \frac{K_p}{Z_c}\left[\frac{1 - R_\infty}{1 + R_\infty}\right] \qquad \textbf{Eq. 4}$$

The probe constant K_p can be determined by measuring the reflections occurring at infinite time in solutions of known electrical conductivity (Zegelin, et al., 1989) or calculated by using Eq. 3 with the impedance of the probe Z_p calculated as in Ball (2002):

$$Z_p = \frac{1}{2\pi n}\sqrt{\frac{\mu_0}{\varepsilon_0}}\, ln\left(H + \sqrt{H^2 - 1}\right) \qquad \textbf{Eq. 5}$$

with

$$H = \frac{(s^2 - a^2)^n - a^{2n}}{a^n((s + a)^n - (s - a)^n)} \qquad \textbf{Eq. 6}$$

where μ_0 is the magnetic permeability in vacuum ($1.26 \cdot 10^{-6}$ N A^{-2}), ε_0 is the permittivity of free space, a is the radius of the single conductor (mm), s is the spacing between conductors (mm) and n is the number of external conductors (n=2 for trifilar probe). The nominal value of the probe constant K_p is also often provided by the manufacturer.

3.1.2 Signal correction

Correction of the TDR signal is needed when the reflection measured in air is not equal to the theoretical value of 1 and when the reflection measured on the short circuited probe is not equal to the theoretical value of -1. Castiglione & Shouse (2003) have suggested calculating a corrected reflection coefficient $R_{\infty,c}$ to account for additional losses in the system as follows:

$$R_{\infty,c} = \frac{R_{air} - R_{\infty}}{R_{\infty} - R_{sc}} \qquad \textbf{Eq. 7}$$

where R_{∞} is the reflection coefficient at infinite time, R_{air} is the reflection coefficient measured in air and R_{SC} is the reflection coefficient measured on the short-circuited probe. If $R_{\infty,c}$ is substituted for R_{∞}, the conductivity of the sample can finally be calculated from Eq. 4 as follows:

$$\sigma = \frac{K_p}{Z_c}\left[\frac{1 - R_{\infty,c}}{1 + R_{\infty,c}}\right] \qquad \textbf{Eq. 8}$$

The electrical resistivity ρ is the reciprocal of the electrical conductivity σ, so it can be calculated as:

$$\rho = \frac{1}{\sigma} \qquad \textbf{Eq. 9}$$

3.1.3 Calibration of the resistivity function

Two 75 mm long TDR probes with three rods were used for the measurements. The TDR probes (Campbell Scientific CS640) were calibrated to establish the relationship between the conductivity and the reflection coefficients that the probes return by measuring the reflections occurring at infinite time in sodium chloride (NaCl) solutions of known electrical conductivity. The conductivity of NaCl solutions is related to the molality of the solution (Weast, et al., 1985). Solutions with electrical conductivity ranging between 1,500-12,000 µS/cm were prepared by mixing oven-dried salt and demineralised water in a 120 mm high plastic container having a 100 mm diameter. Preliminary tests were carried out on kaolin samples having the same dimensions to ensure that the TDR measurements were not affected by the container. Tests were carried out by inserting the probe in different positions in the centre and on the edge of the samples and comparing the resistivity values obtained from these measurements. Results showed a maximum difference in resistivity values of 0.2 Ωm, thus confirming that the sampling volume has diameter equal to the distance between the outer rods of the probe (Ferre, et al., 1998).

The TDR probe was fully inserted into the solution and the final reflection R_∞ was measured and corrected as shown in Eq. 7 to account for the dissipation of the signal in the cables.

The slope of the calibration curve (Fig. 3) represents the ratio K_p/Z_c (Eq. 8) for each probe. The obtained values are equal to 899 μS/cm and 871 μS/cm respectively. These values derived from the probe-specific calibration were checked against the values derived from the manufacturer specifications (Campbell Scientific, 2006). The probe constant K_p provided by the manufacturer is equal to 6.4 S/m Ω. Assuming a value of Z_c equal to 63.6 Ω for the impedance of the cable, as reported in Tarantino & Pozzato (2008), a value of K_p/Z_c equal to 991 μS/cm is obtained, which compares favourably with the measured value.

Moreover, the probe impedance Z_p was calculated using Eq. 5 and a value of 183 Ω was obtained (for s=7.705 mm and a=0.795 mm). By substituting this value in Eq. 3 and considering the same value of Z_c equal to 63.6 Ω, a value of K_p/Z_c equal to 1018 μS/cm was found, which again compares favourably with the value measured from the specific calibration.

3.2 Experimental procedure

3.2.1 Sample preparation

Three cylindrical intact samples 100 mm high, 75 mm diameter were taken at depths of 6.0, 6.5 and 6.6 m from the crest of the embankment.

A 1 cm high slice of each sample was cut and oven-dried to estimate the initial volumetric water content, which was equal to 0.31, 0.46 and 0.52 for the samples taken at depths of 6.0, 6.5 and 6.6 m respectively. Samples were air-dried in steps and the mass of water evaporated upon each step was used to calculate the volumetric water content reached at the end of each evaporation step. This water content θ_{Target} is given by:

$$\theta_{Target} = \frac{m_w}{\gamma_w V_c} \qquad \textbf{Eq. 10}$$

where m_w is the mass of water in the sample at the time of measurement, γ_w is the unit weight of water at 20°C and V_c is the volume of the cylindrical sample. The samples did not exhibit shrinkage during the air-drying process.

After each evaporation step each sample was sealed in a plastic bag for 24 hours to let the water content homogenise before taking the TDR measurement. The TDR probe was initially slowly pushed centrally into the sample to avoid deforming the probe rods and it was left in the sample for all measurements.

Loose material collected from the embankment at a depth between 3 m and 4.5 m was used to prepare eleven samples which were compacted to a target value of dry density of 1.52 g/cm^3 to replicate the dry density in the field (Amabile, et al., 2020). The samples were prepared with target volumetric water contents θ_{Target} ranging between 0.14 and 0.32, calculated as:

$$\theta_{Target} = \rho_{dry} \frac{m_w}{m_s} \gamma_w \qquad \textbf{Eq. 11}$$

where ρ_{dry} is the dry density and m_w and m_s are respectively the mass of water and the mass of soil used to prepare the sample.

Samples were prepared by mixing the oven dried soil with fluids at different conductivities σ_w to evaluate the influence of the fluid on the bulk electrical resistivity. In particular, demineralised water, NaCl solution mimicking electrical resistivity of the Adige River, and NaCl solution having electrical resistivity much higher than the Adige River were considered. The Adige-like solution was prepared by measuring the electrical conductivity of the water collected from the Adige River and reproducing similar electrical conductivity by adding NaCl to demineralised water. Details about the preparation of the samples are reported in Table 1.

For each sample, the dry soil was spread on a tray in a thin layer, sprayed with water and mixed carefully to avoid the formation of lumps. To obtain a uniform value of water content the samples were prepared in two steps. Half of the soil was spread in a thin layer (~1 mm) and wetted with half of the amount of water; after mixing, the second half of soil was added on the tray, wetted with the remaining water and mixed with the first half sample. Each sample was left in a sealed plastic bag for 24 hours to let the water content homogenise.

The samples were compacted in a mould having diameter equal to 100 mm and height equal to 120 mm. For the compaction each sample was divided in three equal parts. Each part was put in the mould and compacted until the layer reached the required thickness of 40 mm. The samples were compacted with a standard compaction hammer, having weight equal to 4.5 kg and a drop of 457 mm. TDR measurements were taken on each sample immediately after compaction and then the samples were discarded in order to keep under control the salt concentration and therefore fluid conductivity for each sample.

Table 1 - Compacted samples prepared at different target water contents θ_{Target} and with pore water having different electrical conductivity σ_w.

Sample	θ_{Target}	Water	σ_w [S/m]
D1	0.14	Demineralised	0.00005
D2	0.21	Demineralised	0.00005
D3	0.32	Demineralised	0.00005
A1	0.16	Adige-like	0.02
A2	0.26	Adige-like	0.02
A3	0.21	Adige-like	0.02
A4	0.32	Adige-like	0.02
A5	0.15	Adige-like	0.02
A6	0.25	Adige-like	0.02
S1	0.15	Saline	0.10
S2	0.25	Saline	0.10

3.2.2 Water content

For every measurement the water content was determined as in Topp, et al. (1980):

$$\theta_{Topp} = -5.3 * 10^{-2} + 2.92 * 10^{-2} K_a - 5.5 * 10^{-4} {K_a}^2 + 4.3 * 10^{-6} {K_a}^3 \qquad \textbf{Eq. 12}$$

where K_a is the apparent dielectric permittivity of the sample. The value of K_a was obtained from the propagation velocity of the pulse in the probe as described in Tarantino et al. (2008):

$$K_a = \left(c\frac{t_{end} - t_{probe}}{2L_e}\right)^2 = \left(c\frac{t_{end} - (t_{head} + \Delta t)}{2L_e}\right)^2 \qquad \textbf{Eq. 13}$$

where L_e is the electrical length of the probe (m), c is the speed of light ($3 \cdot 10^9$ m s^{-1}), t_{end} is the time corresponding to the reflection at the end of the rods (s), t_{probe} is the time at which the wave enters the probe electrodes (s), t_{head} is the time at which the wave enters the head of the probe (s) and Δt is the time interval between t_{head} and t_{probe}. The values of L_e and Δt were obtained from the probe calibration in air and water (Robinson, et al., 2003), while the times t_{end} and t_{head} were obtained graphically from the waveform in terms of reflection coefficient as shown in Fig. 4. The time t_{head} corresponds to the first dip in the waveform signal, while the time t_{end} can be found at the intersection point between the tangent to the second rising limb at the inflection point and the horizontal tangent at the base of the signal (Baker & Allmaras, 1990).

The volumetric water content calculated using Topp's equation was compared to the imposed water content θ_{Target} for the compacted samples and a good agreement was found as shown in Fig. 5. Intact samples are not included in Fig. 5 because the measurement of the volumetric water content was affected by inaccuracies in the measurement of the total volume after extrusion from the sampler.

3.2.3 Relationship between resistivity and water content

The electrical resistivity of a porous medium depends on its moisture content. The resistivity and the volumetric water content of an unsaturated soil can be related via Archie's law (1942) as:

$$\rho = k \cdot n^{-p} \cdot {S_r}^{-m} \qquad \textbf{Eq. 14}$$

where ρ is the electrical resistivity of the unsaturated soil, n is the porosity, S_r is the degree of saturation and k, p and m are coefficients depending on the type of soil, with k also dependent on the resistivity of the fluid in the pores. Experimental evidence has shown that the fitting parameters p and m can be assumed to have the same value, leading to the formulation of the generalised Archie's law (Shah & Singh, 2005), which can be used to relate electrical resistivity to volumetric water content θ as follows:

$$\theta = \alpha\rho^{-\beta} \qquad \textbf{Eq. 15}$$

For both the intact and compacted samples the values of the fitting parameters α and β were found by plotting the measured resistivity against the volumetric water content calculated with Eq. 12 and fitting the data points with the expression in Eq. 15. The results are shown in Fig. 6.

The data points corresponding to samples prepared with demineralised water show a larger value of resistivity at the same water content compared to samples prepared with saline water. This trend is consistent with expectations, being the conductivity of the demineralised water much lower than the one of the saline water. However, when comparing the data points corresponding to the resistivity of the Adige River to the ones corresponding to saline water, no significant difference can be observed as both sets of data points align on the same curve. This shows that although the different resistivity of the fluid in the pores plays a role in the measured bulk resistivity, its effect is not proportional to the difference in the resistivity of the fluid on its own. This is reasonably associated with the electrical interaction between clay particles and ions in the water. The difference in the resistivity values measured for the compacted samples is comparable to the scattering in the data points corresponding to measurements taken on intact samples, which is only generated by the natural variability of the soil in the samples. For this reason all the experimental data points were fitted by the same power function with α=4.166 ($\Omega^{-1}m^{-1}$) and β=0.622.

4 ERT data

4.1 Field measurements

Electrical resistivity tomography (ERT) is based on the measurement of resistivity in the soil using a large number of electrodes placed at the ground surface. 2D ERT measurements were taken in two surveying campaigns on the Adige River embankment. The first campaign was carried out in the wet season and one week after a moderate flood (autumn 2014), while the second campaign was carried out during the dry and warm season (summer 2015). The river levels recorded during both surveying campaigns are shown in Fig. 1. The surveys were aimed at mapping the water content in the unsaturated zone above the phreatic surface.

Measurements were taken along the longitudinal and cross-sectional profile of the embankment. For the longitudinal profile, electrodes were installed on the crest of the embankment along a 50 m segment (chainage km 122.415-122.460) with 1 m spacing between the electrodes. For the cross-sectional profiles, electrodes were installed along the topographic profile of the embankment in a 40 m long array, starting from the river level on the riverside and progressing towards the toe of the embankment, with an electrode spacing of 1.5 m as shown in Fig. 1. Measurements were taken along three cross-sections located at chainage km 122.425, km 122.445 and km 122.452, as shown on the map in Fig. 7. A Schlumberger array configuration was chosen for the ERT measurements and the device ARES (GF Instruments, Czech Republic) was used. The maximum penetration depth from the crest of the embankment is about 10 m, therefore allowing measuring the resistivity in the entire unsaturated zone in the embankment core and also below the phreatic surface.

4.2 Resistivity from ERT measurements

2D resistivity profiles were compiled using the programme Res2Dinv (GEOTOMO Software - Malaysia). Data points with out-of-range values of resistivity were removed from the measured datasets before the inversion. These values were associated with inadequate electrode grounding, i.e. anomalous electrode contact resistance on the asphalt cover on the crest. The proportion of the excluded data did not exceed 5% of the total data at any of the measured profiles. The robust least-square inversion method was selected because a sharp contrast in resistivity was expected between the gravelly shell layer and the silty material in the core of the embankment (Loke & Barker, 1995). The RMS error at the 5th iteration was considered acceptable (<10%) for all the measurements. The topographic profile was included in the modelling mesh. Examples of resistivity contours obtained from the inversion are shown in Fig. 8 for one representative cross section. The areas of high resistivity close to the ground surface below the crest of the embankment correspond to the shell layer which is made of gravelly material. The pavement on the crest of the embankment prevents infiltration of water from the surface, leading to a very high resistivity in the dry gravel. This is more evident during summer because on the sloping sides of the embankment the shallow layer is also dry due to evaporation. The high resistivity at the toe of the berm on the landside is associated to a drainage system. For depths greater than 7 m the material shows a uniform resistivity in the range 50-100 Ωm. This resistivity is associated to the saturated foundation material.

4.3 Effect of temperature

The resistivity values were corrected to account for temperature changes in the subsurface soil due to seasonal variations according to Eq. 16 (Keller & Frischknecht, 1966):

$$\rho_{20} = \rho \cdot \left(1 + b(T - 20°)\right) \qquad \textbf{Eq. 16}$$

where ρ_{20} is the resistivity at a reference temperature of 20°C, ρ is the resistivity obtained from the inversion of the ERT data, b is taken equal to 0.02 °C^{-1} (Hayley, et al., 2007) and T is the temperature in the subsurface soil (°C).

Temperature variations in the subsoil can be described by the following equation (Kasuda & Archenbach, 1965):

$$T(t,z) = T_m - T_a e^{\left(-z\sqrt{\frac{\pi}{365D}}\right)} \cos\left(\frac{2\pi}{365}\left(t - t_s - \frac{z}{2}\sqrt{\frac{365}{\pi D}}\right)\right) \qquad \textbf{Eq. 17}$$

where T is the temperature at time t (expressed in days of the year) and depth z, T_m is the yearly mean temperature at ground surface, T_a is the amplitude of the yearly temperature variation at ground surface, t_s is the phase offset i.e. the day of the year corresponding to the minimum yearly temperature (Table 2). D is the soil's thermal diffusivity which can be calculated as:

$$D = \frac{K}{\rho_s C} \qquad \textbf{Eq. 18}$$

where ρ_s is the average soil density (kg m^{-3}), C the soil specific heat capacity (J kg^{-1} K^{-1}) and K the soil thermal conductivity (W m^{-1} K^{-1}). These parameters change with the water content in the soil, which is not known a priori, therefore an average value was assumed between the values of dry soil and fully saturated soil as reported in the literature (Pal Arya, 2001). The temperature profiles in the subsurface soil obtained for both surveying campaigns are shown in Fig. 9. Although the temperature at ground surface is significantly different for the two seasons, temperature in the subsurface tends to level towards the annual mean temperature of 13°C and the effect of seasonal variations does not affect the temperature in the subsoil for depths greater than 10 m.

Table 2 – Yearly temperature data for San Floriano in 2014 and 2015 (Autonomous Province of Bozen, 2018).

	2014 (autumn)	*2015 (summer)*
T_m [°C]	13.9	13.8
T_a [°C]	13.6	15.9
t_s [day]	360	32
t_{ERT} [day]	316	175

The average corrected resistivity profile below the crest of the embankment is shown in Fig. 10 for one representative cross-section. For ease of comparison the soil profile is also shown in the same figure, where the shaded areas at the top and the bottom of the profile represent the gravelly shell and foundation material respectively. Resistivity at a given depth is the average measured across the crest footprint. The values of corrected resistivity in summer are much higher than the ones measured in autumn at shallow depths. This appears to be consistent with a lower phreatic surface, which generates higher suction and, hence, lower water contents. At greater depths (below 212 m a.s.l.) no significant difference can be observed between the two seasons and the resistivity has a constant value of about 50 Ωm. This part of the embankment is below the phreatic surface, therefore this value of resistivity is not affected by the moisture content and corresponds to the resistivity measured for the fully saturated material.

5 Inverse analysis of monitoring data

To benchmark the water content profiles obtained from the ERT measurements, numerical simulations of water flow in the embankment at the time of ERT measurements were carried out. Since the three cross-sections where ERT measurements were taken are very close, a single geotechnical model was considered (Fig. 1). The numerical model was calibrated by inverse analysis of the water flow based on the measurements of the piezometers and tensiometers installed in the field. The values of the saturated hydraulic conductivity of the materials in the core of the embankment and in the foundation were obtained from the inverse analysis of the monitoring data (Amabile, et al., 2020). The water retention curve of the embankment core material (Fig. 11) was derived experimentally in the laboratory on specimens collected at different depths (Amabile, et al., 2020), while the unsaturated hydraulic conductivity was derived from the water retention curve using Van Genuchten's model for the relative hydraulic conductivity (Van Genuchten, 1980):

$$k_{rel} = {S_e}^{-0.5}\left(1-\left(1-{S_e}^{\frac{1}{m}}\right)^{m}\right)^{2} \qquad \textbf{Eq. 19}$$

Where k_{rel} is the ratio between unsaturated and saturated hydraulic conductivity, S_e is the effective saturation and $m = 0.305$.

The hydrograph in the water flow simulations is given by the level of the Adige River at the study site, which is recorded by a hydrometer and is shown in Fig. 12 for the months corresponding to the two ERT measurement campaigns. In June 2015 no significant change of the river level was observed in the weeks leading up to the time of ERT measurements, therefore steady-state conditions were considered in the water flow simulations. In November 2014 a moderate flood was observed a few days before the ERT measurements, therefore transient conditions were taken into account in the water flow simulation to account for the variations of river level in the ten days preceding the ERT measurement. Numerical simulations were carried out using the finite element software SEEP/W (GEO-SLOPE, 2004) and more details about the numerical model can be found in Amabile et al. (2020).

6 Discussion

The average resistivity profiles deriving from ERT measurements were converted in volumetric water content profiles using the relationship between resistivity and volumetric water content obtained in the laboratory tests (Fig. 6).

The comparison of water content profiles obtained from the ERT data and from the inverse analysis of monitoring data is shown in Fig. 13 for both seasons.

From a qualitative point of view the comparison between water content profiles shows a good match between the water contents derived from ERT and the numerical simulation of water flow. The profiles show the same trend, with increasing water content with depth in the unsaturated area and a constant water content, corresponding to the saturated one, in the saturated zone.

However, from a quantitative point of view the water content obtained from ERT data does not seem to give an accurate estimate of the water content in the embankment. The water content derived from ERT measurement is always lower than the one obtained from numerical simulations, meaning that the resistivity returned by the inversion of the ERT data is greater than the one obtained from TDR measurements in the laboratory. This may be due to artefacts associated to the inversion process. The high contrast in resistivity between layers has been acknowledged as a source of artefacts during the inversion in several applications ((Carey, et al., 2017); (Hilbich, et al., 2009); (Rings, et al., 2008)), raising questions about the reliability of resistivity values obtained in the areas of the model where such contrasts are found. For the embankment in San Floriano, the resistivity returned by the inversion in the gravelly shell layer reaches values as high as 2200 Ωm in autumn and 3500 Ωm in summer. The high contrast between the resistivity of the gravelly shell and the resistivity of the silty material in the embankment core may therefore be the source of the mismatch observed in terms of water content.

The mismatch is more evident for the summer measurement, when the evaporation from ground surface is more intense and leads to a very dry gravelly shell layer. The higher contrast in resistivity values at the boundary between the two layers would explain why the difference between the ERT derived water content and the one obtained from the inverse analysis of monitoring data is more significant for measurements taken during summer.

This issue can be addressed by deriving a field specific relationship between the resistivity returned by the inversion of ERT data and the water content. This can be achieved by having an independent measurement of water content at the same time as the ERT measurement to relate the two variables (Fan, et al., 2015). To test this approach, a field specific water content-resistivity relationship was derived using the average resistivity profile obtained from the longitudinal ERT measurements carried out on the crest of the embankment in the first measurement campaign (autumn 2014). This resistivity profile was associated to the water content profile obtained from the numerical simulations based on the inverse analysis of monitoring data. The field specific relationship is shown in Fig. 14 together with the curve obtained from the laboratory testing. The two curves diverge significantly for values of resistivity higher than 100 Ωm, with the field-derived curve showing much higher values of water content corresponding to the same resistivity.

The field specific water content- resistivity relationship built on the autumn 2014 dataset was then validated against its capability to simulate the water content on the summer 2015. To this end, the field specific water content- resistivity relationship was used to convert the resistivity profiles obtained from the ERT on the cross section for the summer 2015 campaign. As shown in Fig. 15, there is a satisfactory quantitative prediction of the ERT-based water content compared with the one derived from the water flow analysis.

The same figure also shows the water content profile derived from the ERT on the cross section in the autumn 2014 campaign. The good match with the water content derived from the water flow analysis is trivial because essentially these same ERT data have been used to construct the water content - resistivity relationship.

These results show that ERT may be a suitable method to capture the soil's volumetric water content not only qualitatively, but also from a quantitative point of view. If a direct or indirect measurement of water content is used to calibrate a field-based relationship between the ERT derived resistivity and the water content, ERT can be successfully used to determine water content profiles in the subsoil.

7 Conclusions

The paper has presented an application of ERT technique to assess water content in a flood embankment on the Adige River, where a monitoring system consisting of piezometers and tensiometers is installed. The relationship between water content and resistivity expressed by Archie's law has been characterised in the laboratory using TDR on intact and compacted samples collected from the embankment. This allowed converting the temperature-corrected resistivity profiles derived from ERT measurement along the cross section of the embankment into water content profiles.

Data from the monitoring system have been used to calibrate a numerical model to analyse water flow in the embankment via inverse analysis. Comparison of ERT-derived water content profiles with water content profiles derived from water flow simulations has shown that ERT can capture the qualitative trend of water content variations in the embankment. However, the high resistivity contrasts between the silty material in the core of the embankment and the gravelly shell layer on the top surface can affect the quantitative interpretation of the results. When there are strong contrasts in the ERT derived resistivity profiles the results tend to be less reliable because of artefacts generated by the inversion process. In this case, an experimental field-calibrated relationship between resistivity and water content can be developed in order to obtain a satisfactory quantitative assessment of the water content. This can be achieved by coupling ERT with more traditional geotechnical monitoring systems based on the use of local sensors, to have an initial direct or indirect measurement of water content in the field.

ERT has proven to be a quick and cost effective tool to assess the water regime in earth structures such as flood embankments. This technique can be easily applied to identify patterns of water flow and anomalies in the moisture content in the soil, which in turn can provide valuable information about the stability of flood embankments.

Acknowledgements

The authors wish to acknowledge the support of the European Commission via the Marie Curie Industry-Academia Partnership and Pathways Network MAGIC ‘Monitoring systems to Assess Geotechnical Infrastructure subjected to Climatic hazards’ (PIAPP-GA-2012-324426). The authors also wish to acknowledge the support of the Autonomous Province of Bolzano (Italy).

Captions of Figures

Fig. 1 - Cross-section of the embankment with field instruments and samples collected for material characterisation.

Fig. 2 - Grain size distribution for two loose samples collected from the embankment core at a depth of 3.3m.

Fig. 3 - Calibration curves for the two TDR probes.

Fig. 4 - Typical waveform signal returned by TDR in terms of reflection coefficient R.

Fig. 5 - Comparison between volumetric water content calculated using Topp's equation θ_{Topp} and estimated volumetric water content θ_{Target}. The dashed line denotes a perfect 1:1 relationship.

Fig. 6 - Relationship between resistivity and volumetric water content.

Fig. 7 - Plan view of the study area.

Fig. 8 - Resistivity contours obtained from the inversion of ERT data at chainage km 122.425 in (a) autumn and (b) summer.

Fig. 9 - Temperature profiles in the subsurface at the time of ERT measurements.

Fig. 10 - Average corrected resistivity profile for the cross-section at chainage km 122.425 in summer 2015 and autumn 2014.

Fig. 11 - Water retention curve of the material in the embankment core, after (Amabile, et al., 2020).

Fig. 12 - River level variations recorded in the months of the ERT measurement campaigns.

Fig. 13 - Volumetric water content profiles obtained from ERT data (θ_{ERT}) and from inverse analysis of monitoring data (θ_{MD}) in (a) autumn and (b) summer.

Fig. 14 - Relationship between resistivity and volumetric water content derived from laboratory measurements and from inversion of ERT data.

Fig. 15 - Volumetric water content profiles obtained from ERT data (θ_{ERT}) and from inverse analysis of monitoring data (θ_{MD}) using a field specific relationship between resistivity and water content in (a) summer and (b) autumn.

References

Amabile, A., Pozzato, A. & Tarantino, A., 2020. Instability of flood embankments due to pore water pressure build-up at the toe: lesson learned from the Adige river case study. *Canadian Geotechnical Journal,* Volume awaiting publication.

Aning, A. A., Tucholka, P. & Danuor, S. K., 2013. 2D Electrical Resistivity Tomography (ERT) Survey using the Multi-Electrode Gradient Array at the Bosumtwi Impact Crater. *Journal of Environmental and Earth Science,* 3(5), pp. 12-27.

Archie, G. E., 1942. Electrical Resistivity Log as an Aid in Determining Some Reservoir Characteristics. *Transactions of the American Institute of Mining and Metallurgical Engineers,* Volume 146, pp. 54-62.

Autonomous Province of Bozen, 2018. *Weather South Tyrol Historical Data.* [Online] Available at: http://weather.provinz.bz.it/historical-data.asp [Accessed March 2018].

Baker, J. & Allmaras, R., 1990. System for automating andmultiplexing soil moisture measurement by time-domain reflectometry. *Soil Sci Soc Am J,* 54(1), pp. 1-6.

Ball, J., 2002. Characteristic Impedance of Unbalanced TDR Probes. *IEEE TRANSACTIONS ON INSTRUMENTATION AND MEASUREMENT,* 51(3), pp. 532-536.

Banham, S. & Pringle, J. K., 2011. Geophysical and intrusive site investigations to detect an abandoned coal-mine access shaft, Apedale, Staffordshire, UK. *Near Surface Geophysics,* 9(5), p. 483–496.

Brunet, P., Clément, R. & Bouvier, C., 2010. Monitoring soil water content and deficit using ERT - A case study in the Cevennes area, France. *Journal of Hydrology,* Volume 380, p. 146–153.

Campbell Scientific, 2006. *TDR probes Instruction manual,* s.l.: s.n.

Carey, A., Paige, G., Carr, B. & Dogan, M., 2017. Forward modeling to investigate inversion artifacts resulting from time-lapse electrical resistivity tomography during rainfall simulations. *Journal of Applied Geophysics ,* Volume 145, p. 39–49.

Castiglione, P. & Shouse, P., 2003. The effect of ohmic cable losses on time-domain reflectometry measurements of electrical conductivity. *Soil Sci Soc Am J,* Volume 67, p. 414–424.

Chambers, J. et al., 2014. 4D electrical resistivity tomography monitoring of soil moisture dynamics in an operational railway embankment. *Near Surface Geophysics,* Volume 12, pp. 61-72.

Cygal, A., Stefaniuk, M., Kret, A. & Kurowska, M., 2016. The application of electrical resistivity tomography (ERT), induced polarization (IP) and electromagnetic conductivity (EMC) methods for the evaluation of technical condition of flood embankment corpus. *Geology, Geophysics and Environment,* 42(3), p. 279–287.

Fan, J. et al., 2015. Quantifying spatiotemporal dynamics of root-zone soil water in a mixed forest on subtropical coastal sand dune using surface ERT and spatial TDR. *Journal of Hydrology,* Volume 523, p. 475–488.

Ferre, P., Knight, J., Rudolph, D. & Kachanoswki, R., 1998. The sample areas of conventional and alternative time domain reflectometry probes. *Water Resources Research,* Volume 36, p. 2461–2468.

Gance, J. et al., 2016. Permanent electrical resistivity measurements for monitoring water circulation in clayey landslides. *Journal of Applied Geophysics,* Volume 126, p. 98–115.

GEO-SLOPE, 2004. *Seepage Modeling with SEEP/W.* s.l.:GEO-SLOPE International, Ltd..

Geotomo, 2003. *Geoelectrical imaging 2D and 3D.* s.l.:s.n.

Giese, K. & Tiemann, R., 1975. Determination of complex permittivity from thin-sample time domain reflectometry improved analysis of step response waveform. *Adv. Mol. Relax. Processes ,* Volume 7, p. 45–59.

Glendinning, S. et al., 2014. Construction, management and maintenance of embankments used for road and rail infrastructure: implications of weather induced pore water pressures. *Acta Geotechnica,* Volume 9, pp. 799-816.

Gunn, D. et al., 2015. Moisture monitoring in clay embankments using electrical resistivity tomography. *Construction and Building Materials,* Volume 92, p. 82–94.

Hayley, K., Bentley, L., Gharibi, M. & Nightingale, M., 2007. Low temperature dependence of electrical resistivity: Implications for near surface geophysical monitoring. *Geophysical Research Letters,* 34(18).

Hilbich, C. et al., 2009. Applicability of Electrical Resistivity Tomography Monitoring to Coarse Blocky and Ice-rich Permafrost Landforms. *Permafrost and Periglacial Processes ,* 20(3), pp. 269-284.

Hojat, A. et al., 2020. Quantifying seasonal 3D effects for a permanent electrical resistivity tomography monitoring system along the embankment of an irrigation canal. *Near Surface Geophysics.*

Jodry, C. et al., 2019. 2D-ERT monitoring of soil moisture seasonal behaviour in a river levee: a case study. *Journal of Applied Geophysics,* Volume 167, pp. 140-151.

Johansson, S. & Dahlin, T., 1996. Seepage monitoring in an earth embankment dam by repeated resistivity measurements. *European Journal of Engineering and Environmental Geophysics,* 1(3), pp. 229-247.

Kasuda, T. & Archenbach, P., 1965. Earth Temperature and Thermal Diffusivity at Selected Stations in the United States. *ASHRAE Transactions,* 71(1).

Keller, G. & Frischknecht, F., 1966. *Electrical Methods in Geophysical Prospecting.* Oxford: Pergamon Press.

Lebourg, T. et al., 2010. Landslides triggered factors analysed by time lapse electrical survey and multidimensional statistical approach. *Engineering Geology,* Volume 114, p. 238–250.

Leucci, G. & Greco, F., 2012. 3D ERT Survey to Reconstruct Archaeological Features in the Subsoil of the " Spirito Santo " Church Ruins at the Site of Occhiolà (Sicily , Italy). *Archaeology,* 1(1), pp. 1-6.

Lin, C., Hung, Y., Yu, Z. & Wu, P., 2013. Investigation of abnormal seepages in an earth dam using resistivity tomography. *Journal of GeoEngineering,* 8(2), pp. 61-70.

Loke, M. & Barker, R., 1995. Least-Squares Deconvolution of Apparent Resistivity pseudosections. *Geophysics,* 60(6), p. 1682–1690.

Ntarlagiannis, D., Robinson, J., Soupios, P. & Slater, L., 2016. Field-scale electrical geophysics over an olive oil mill waste deposition site: Evaluating the information content of resistivity versus induced polarization (IP) images for delineating the spatial extent of organic contamination. *Journal of Applied Geophysics,* Issue 135, pp. 418-426.

Pal Arya, S., 2001. *Introduction to Micrometeorology.* 2nd edition ed. s.l.:Academic Press.

Ramachandran, K., Tapp, B., Rigsby, T. & Lewallen, E., 2012. Imaging of Fault and Fracture Controls in the Arbuckle-Simpson Aquifer, Southern Oklahoma, USA, through Electrical Resistivity Sounding and Tomography Methods. *International Journal of Geophysics,* pp. 1-10.

Reynolds, J., 2011. *An Introduction to Applied and Environmental Geophysics.* 2nd ed. Oxford, UK: Wiley-Blackwell.

Rings, J., Scheuermann, A., Preko, K. & Hauck, C., 2008. Soil water content monitoring on a dike model using electrical resistivity tomography. *Near Surface Geophysics,* 6(2), pp. 123-132.

Robinson, D. et al., 2003. Considerations for improving the accuracy of permittivity measurement using time domain reflectometry: air-water calibration, effects of cable length. *Soil Sci Soc Am J ,* Volume 67, p. 62–70.

Samouelian, A. et al., 2005. Electrical resistivity survey in soil science: a review. *Soil & Tillage Research ,* Volume 83, p. 173–193.

Shah, P. & Singh, D., 2005. Generalized Archie's Law for Estimation of Soil Electrical Conductivity. *Journal of ASTM International,* 2(5).

Tarantino, A. & Pozzato, A., 2008. Strumenti per il monitoraggio della zona non satura (in Italian). *Rivista Italiana di Geotecnica,* Volume 3, pp. 109-126.

Tarantino, A., Ridley, A. & Toll, D., 2008. Field Measurement of Suction, Water Content, and Water Permeability. *Geotech Geol Eng,* Volume 26, pp. 751-782.

Topp, G., Davis, J. & Annan, A., 1980. Electromagnetic determination of soil water content: measurements in coaxial transmission lines. *Water Resour Res ,* Volume 16, p. 574–582.

Topp, G., Yanuka, M., Zebchuk, W. & Zegelin, S., 1988. Determination of electrical conductivity using TDR: soil and water esperiments in coaxial lines. *Water Resour Res,* 24(7), p. 945–952.

Tresoldi, G. et al., 2019. Long-term hydrogeophysical monitoring of the internal conditions of river levees. *Engineering Geology,* Volume 259.

Van Genuchten, M., 1980. A Closed-form Equation for Predicting the Hydraulic Conductivity of Unsaturated Soils. *Soil Sci. Soc. Am. J.,* Volume 44, pp. 892-898.

Weast, R., Astle, M. & Beyer, W., 1985. *CRC Handbook of Chemistry and Physics.* Boca Raton, Florida: CRC Press, Inc..

Zegelin, S., White, I. & Russel, G., 1989. Improved field probes for soil water content and electrical conductivity measurement using time domain reflectometery. *Water Resour Res,* 25(11), pp. 2367-2376 .

Figure 1

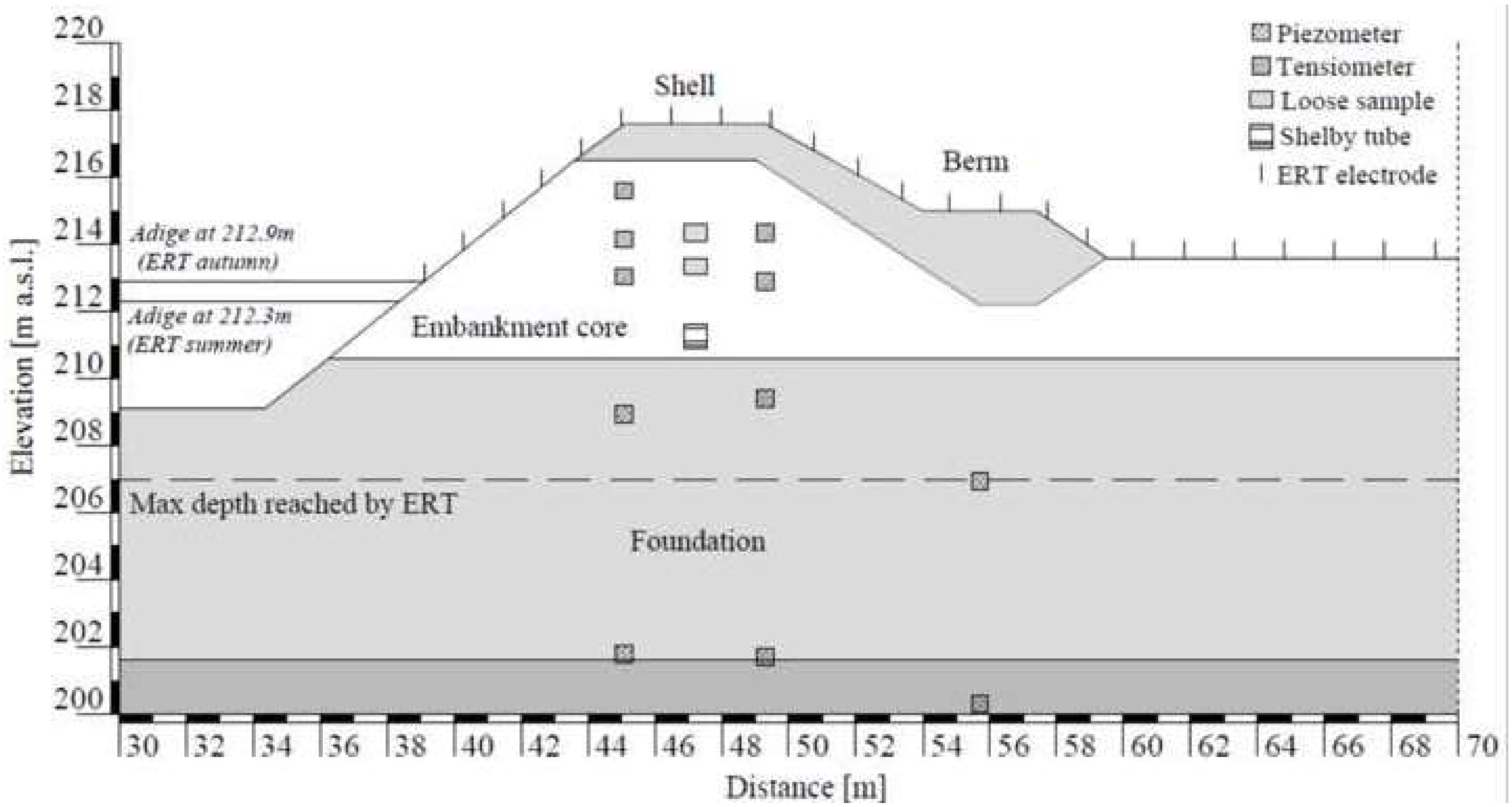
Piezometer
Tensiometer
Loose sample
Shelby tube
ERT electrode
Shell
Berm
Adige at 212.9m
(ERT autumn)
Adige at 212.3m
(ERT summer)
Embankment core
Max depth reached by ERT
Foundation
Elevation [m a.s.l.]
Distance [m]
220
218
216
214
212
210
208
206
204
202
200
30
32
34
36
38
40
42
44
46
48
50
52
54
56
58
60
62
64
66
68
70

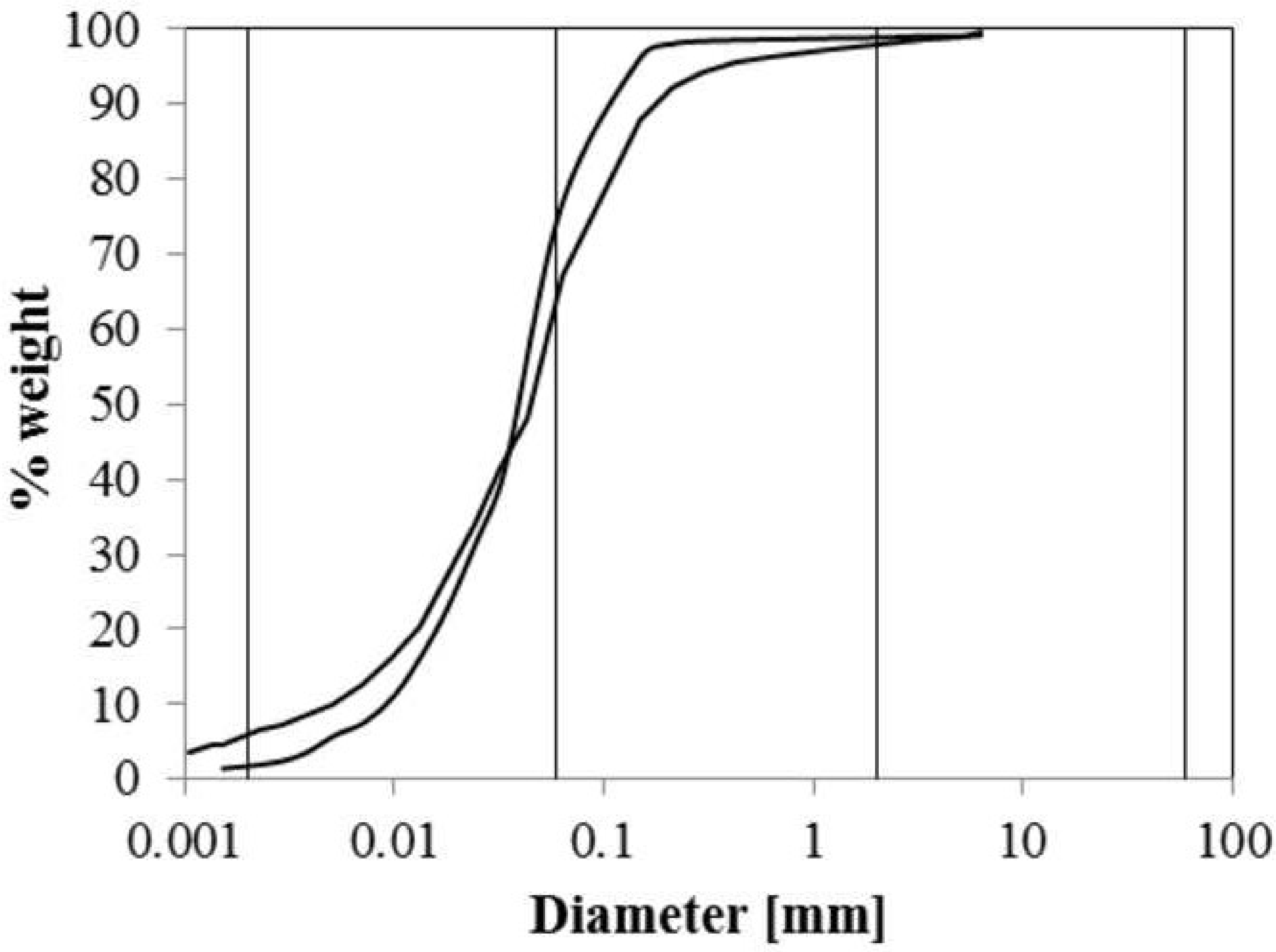

% weight
100
90
80
70
60
50
40
30
20
10
0
0.001
0.01
0.1
1
10
100
Diameter [mm]

Figure

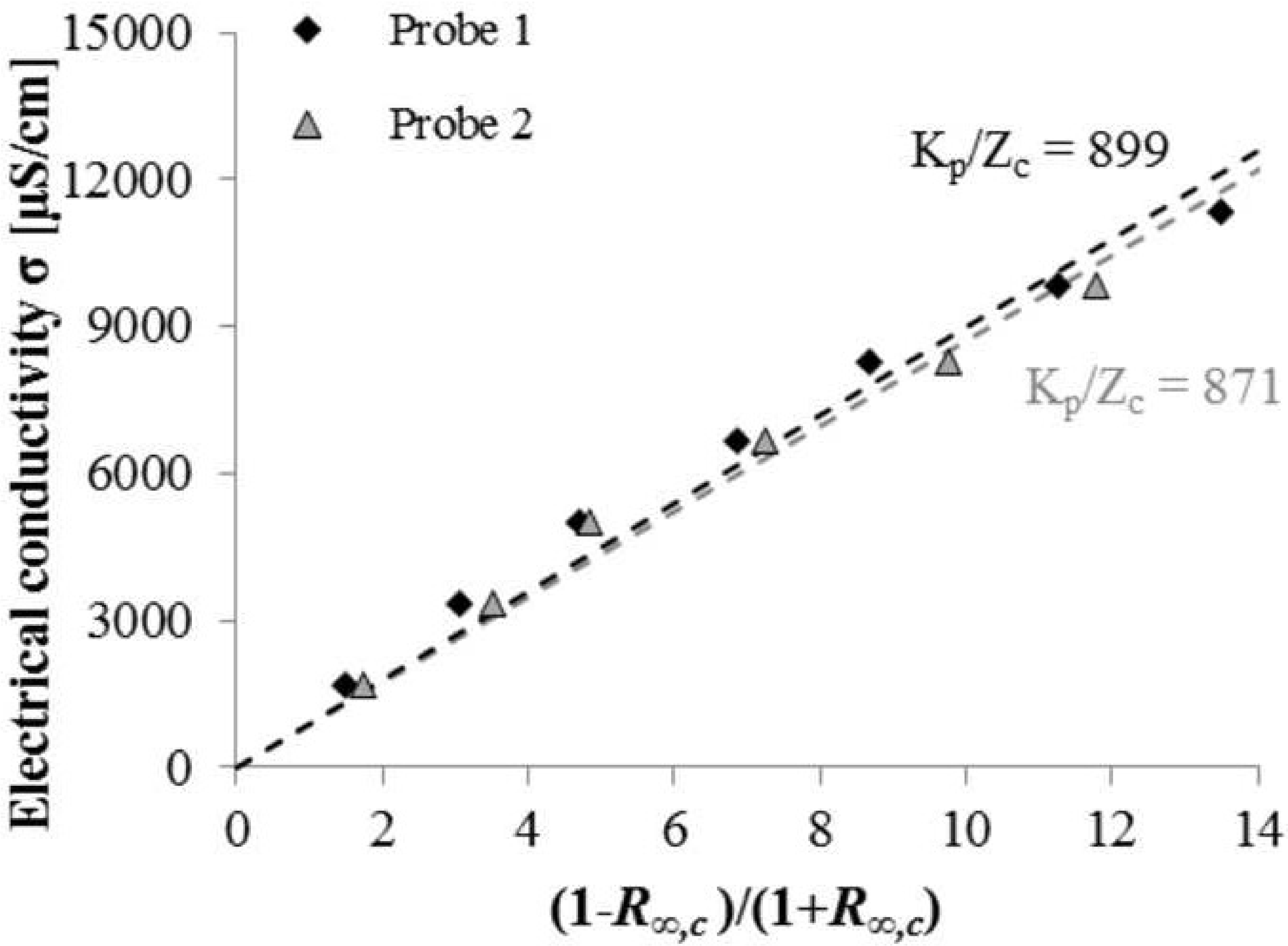

Probe 1
Probe 2
$K_p/Z_c = 899$
$K_p/Z_c = 871$
Electrical conductivity σ [μS/cm]
15000
12000
9000
6000
3000
0
0
2
4
6
8
10
12
14
$(1-R_{\infty,c})/(1+R_{\infty,c})$

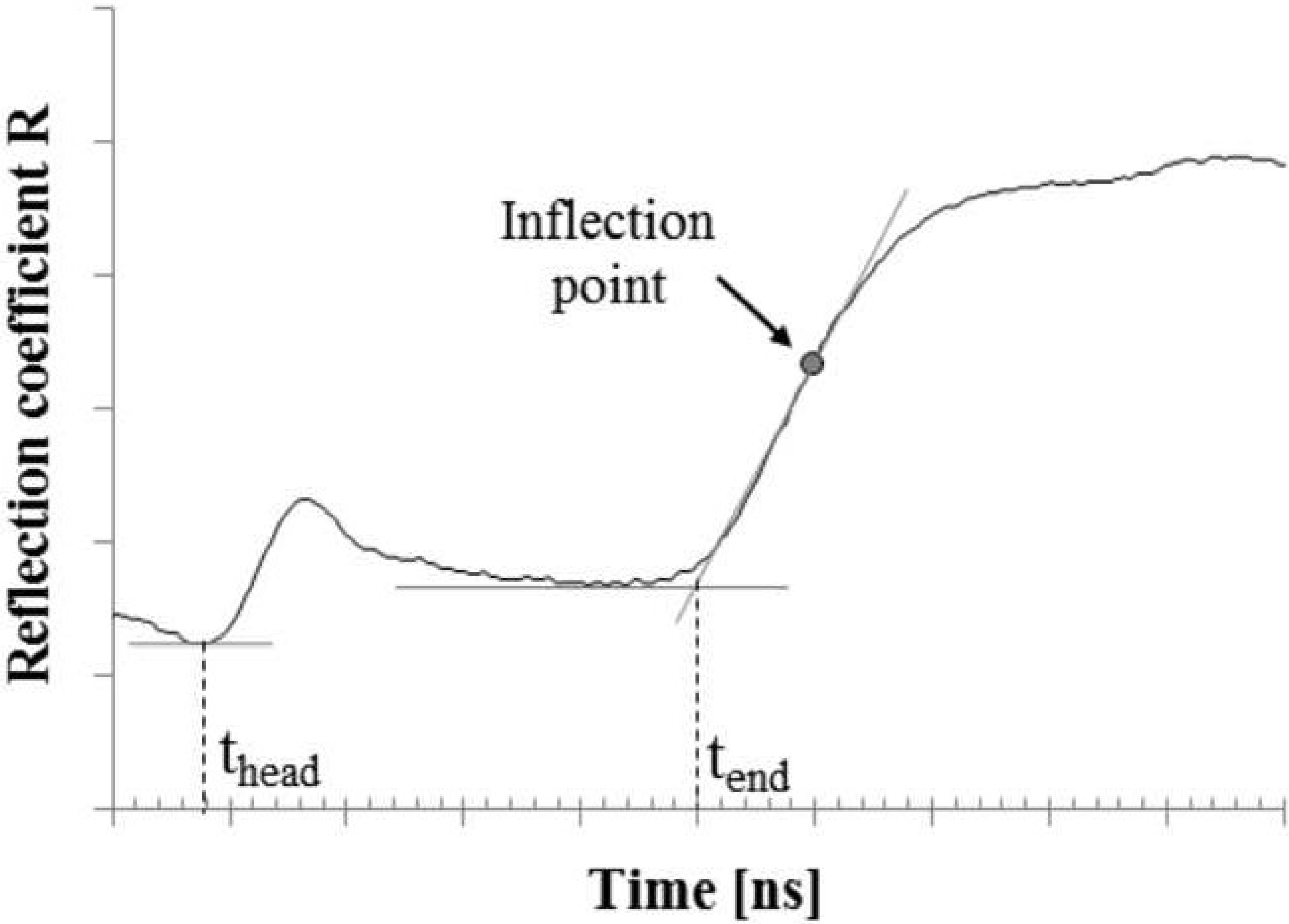

Reflection coefficient R
Inflection point
t_{head}
t_{end}
Time [ns]

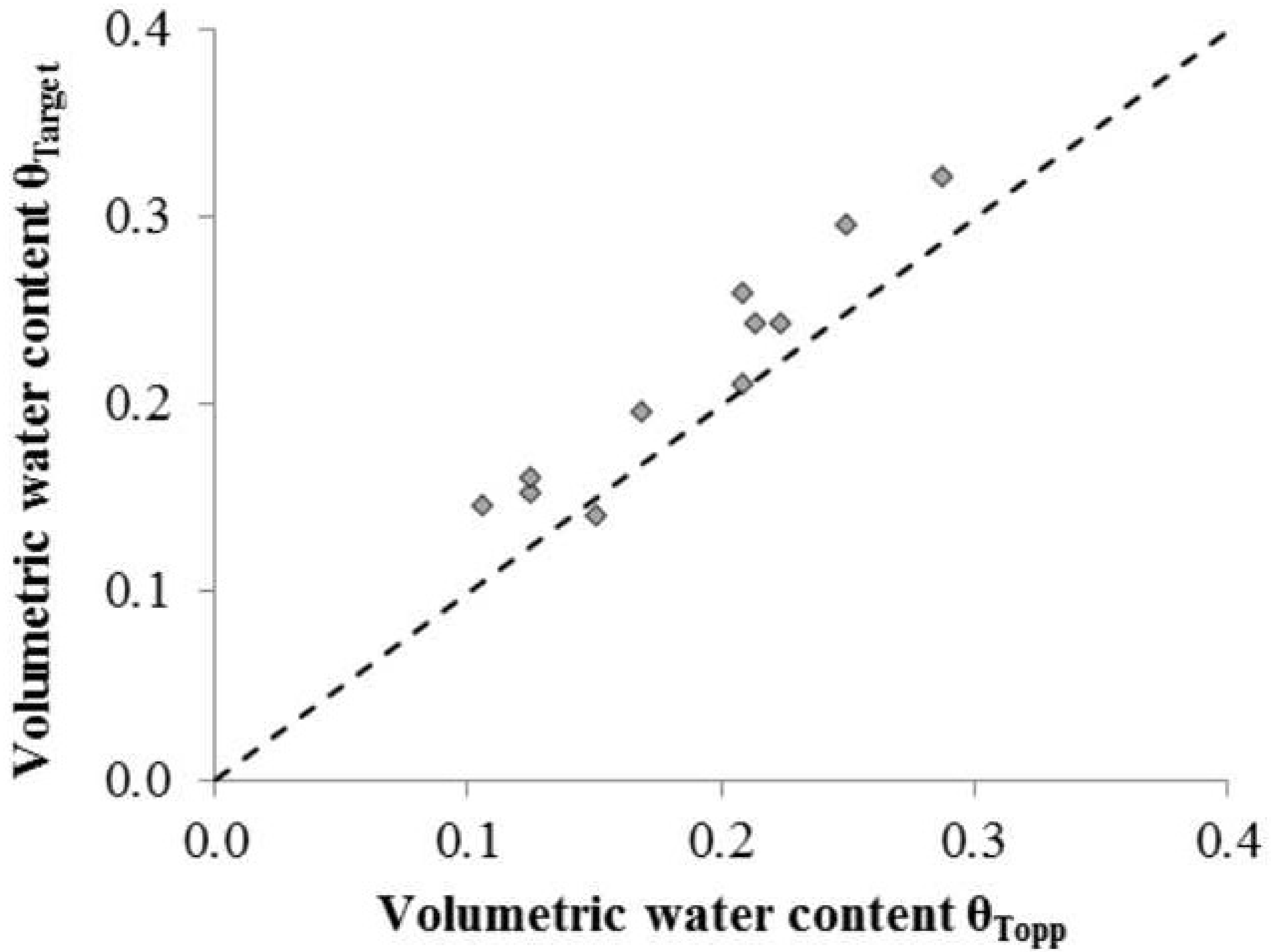
0.4
0.3
0.2
0.1
0.0
0.0
0.1
0.2
0.3
0.4
Volumetric water content θTarget
Volumetric water content θTopp

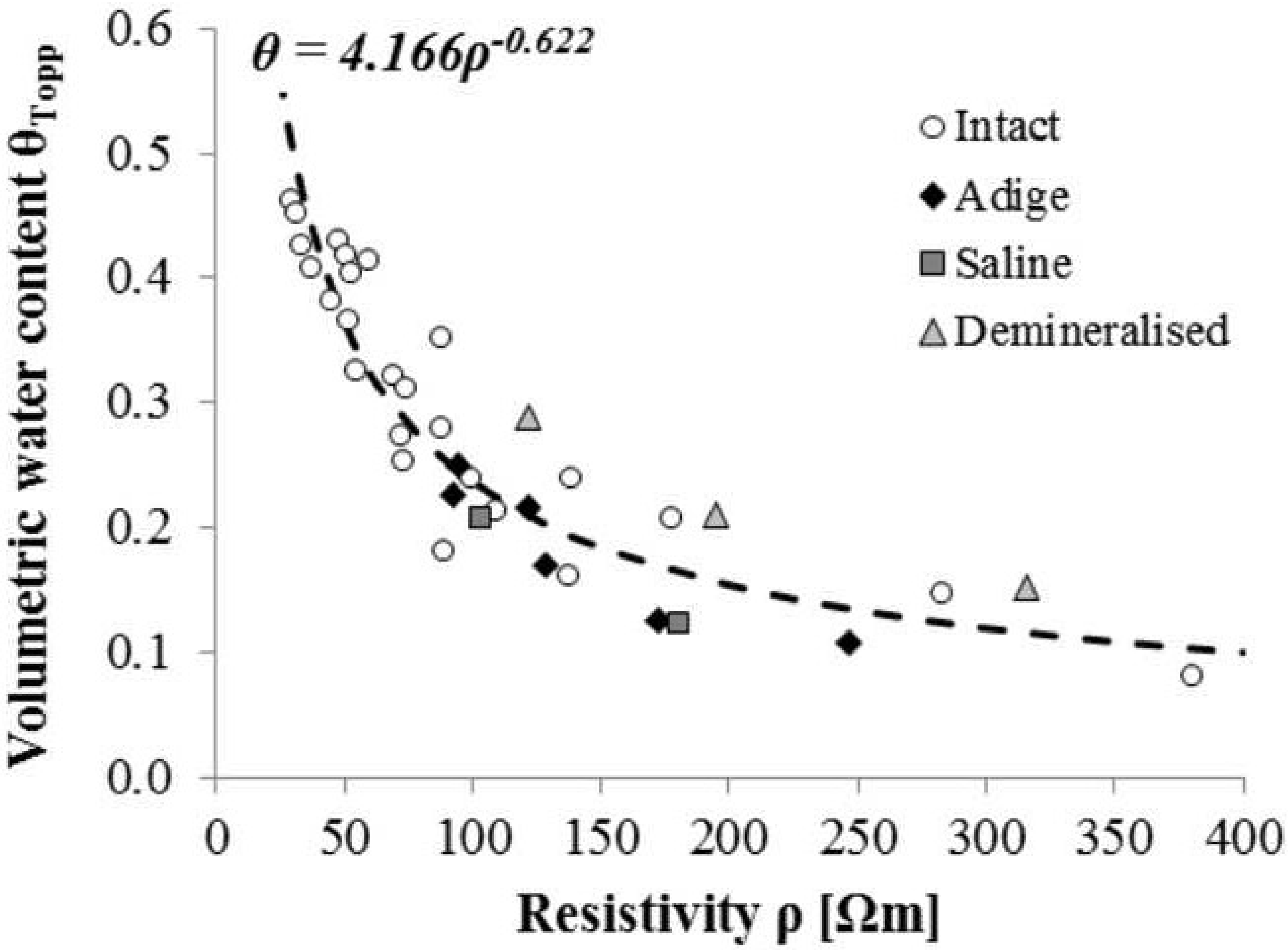

$\theta = 4.166\rho^{-0.622}$
Intact
Adige
Saline
Demineralised
Volumetric water content θ_{Topp}
Resistivity ρ [Ωm]
0.0
0.1
0.2
0.3
0.4
0.5
0.6
0
50
100
150
200
250
300
350
400

Figure

Click here to access/download;Figure;Fig.7.tif

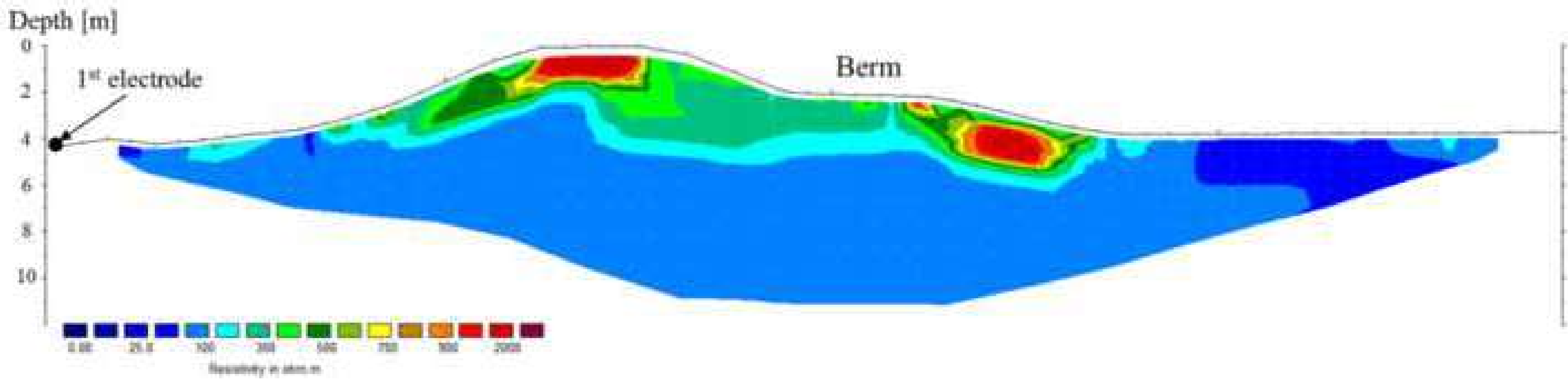
Depth [m]
0
2
4
6
8
10
1st electrode
Berm
0.00
25.0
100
300
500
750
900
2000
Resistivity in ohm.m

Figure

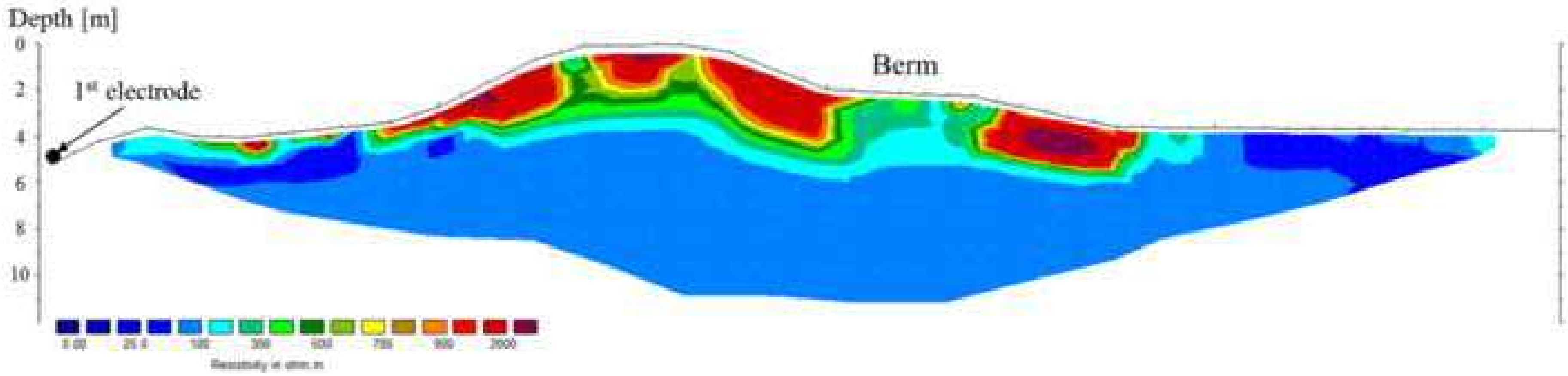

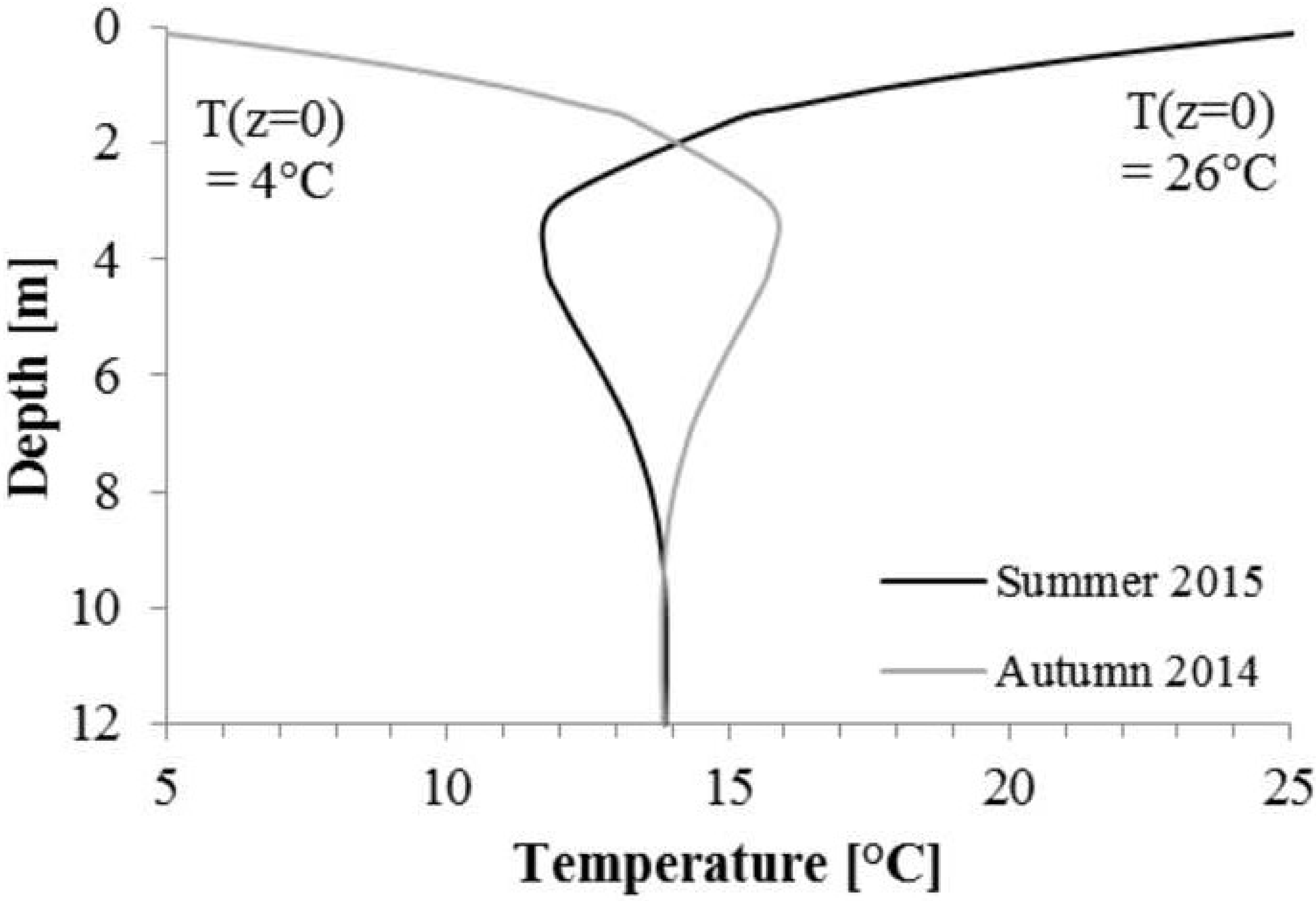
T(z=0)
= 4°C
T(z=0)
= 26°C
Summer 2015
Autumn 2014
Depth [m]
Temperature [°C]
0
2
4
6
8
10
12
5
10
15
20
25

Figure

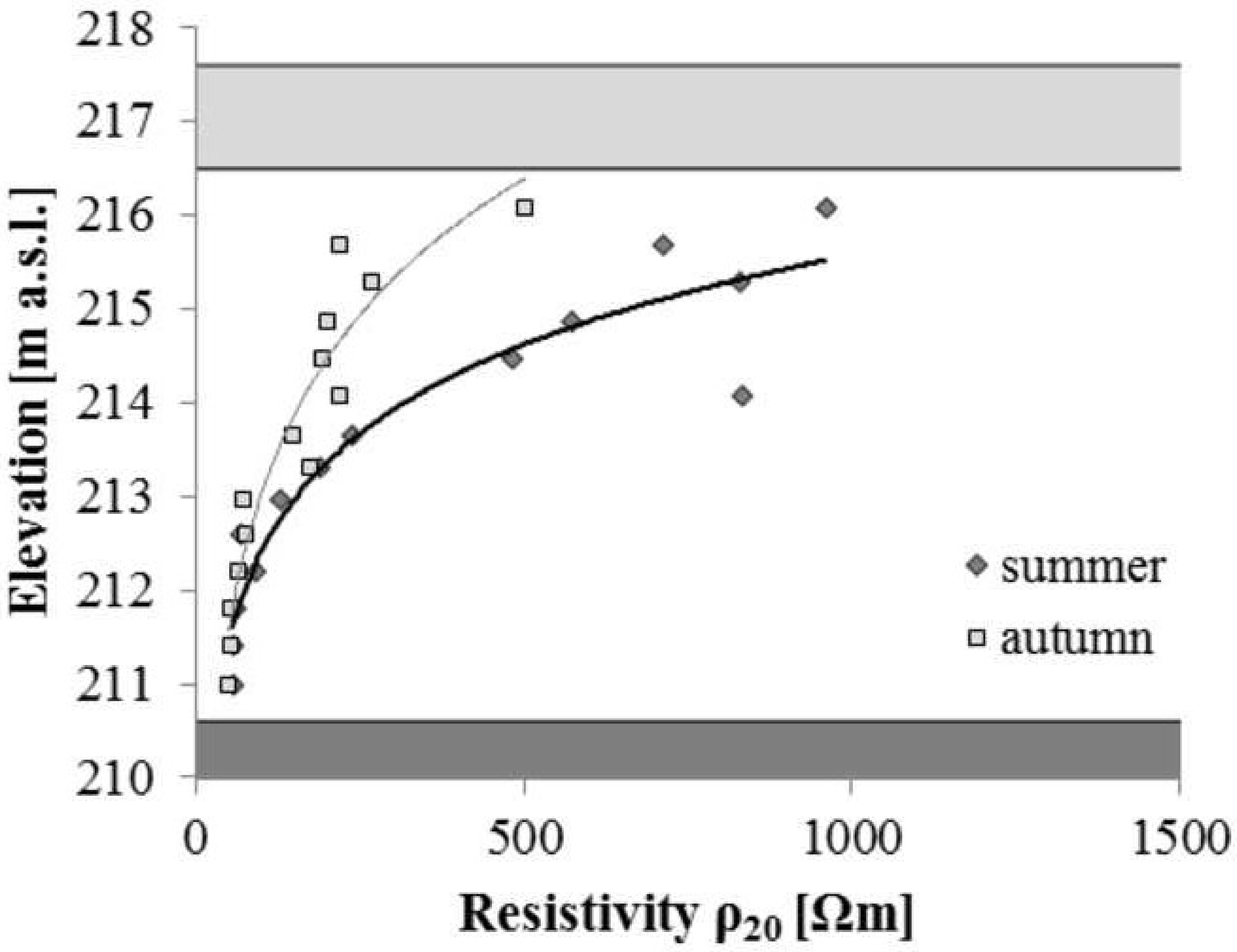

218
217
216
215
214
213
212
211
210
Elevation [m a.s.l.]
0
500
1000
1500
Resistivity ρ20 [Ωm]
summer
autumn

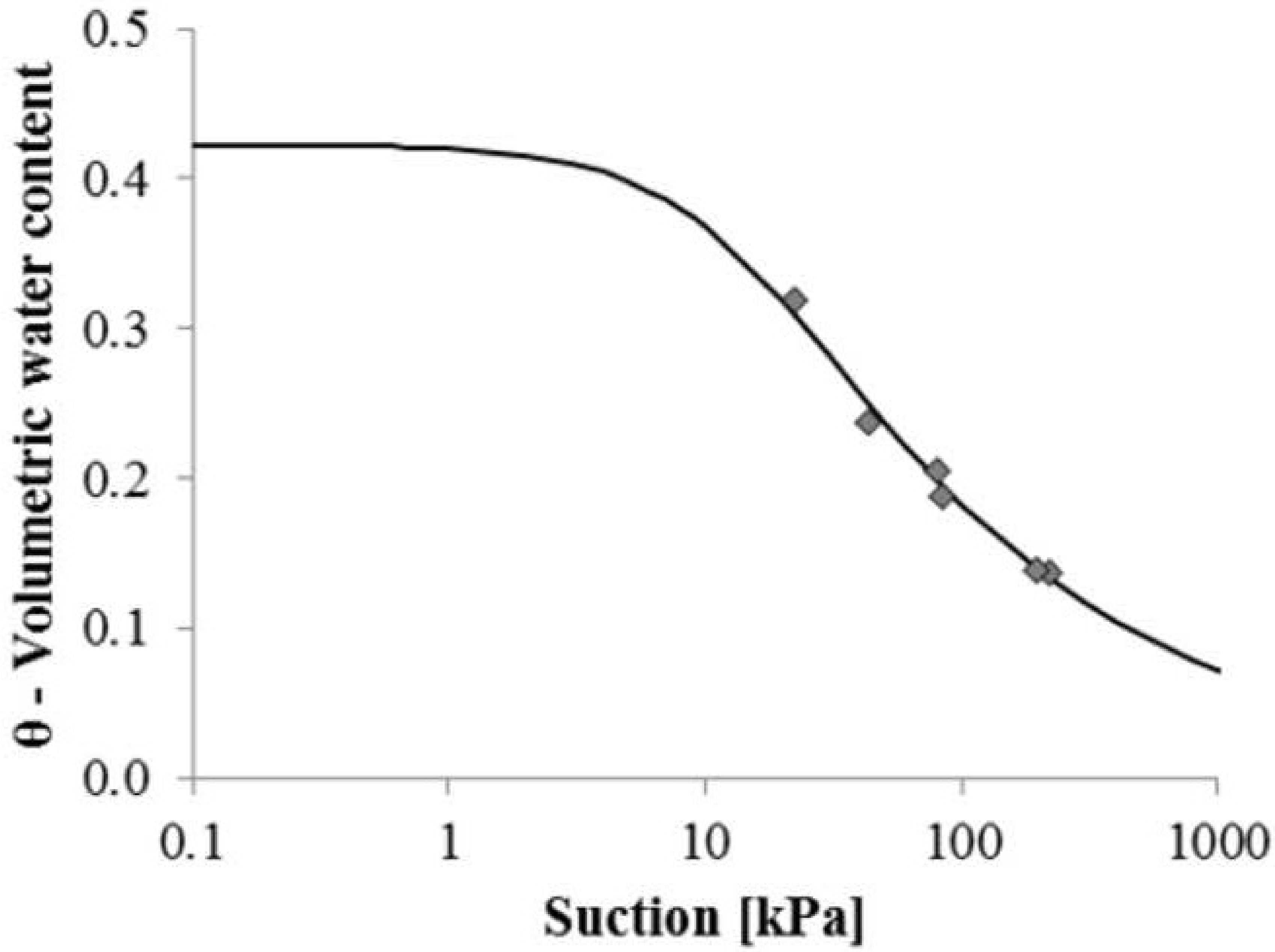
θ - Volumetric water content
0.5
0.4
0.3
0.2
0.1
0.0
0.1
1
10
100
1000
Suction [kPa]

Figure 12

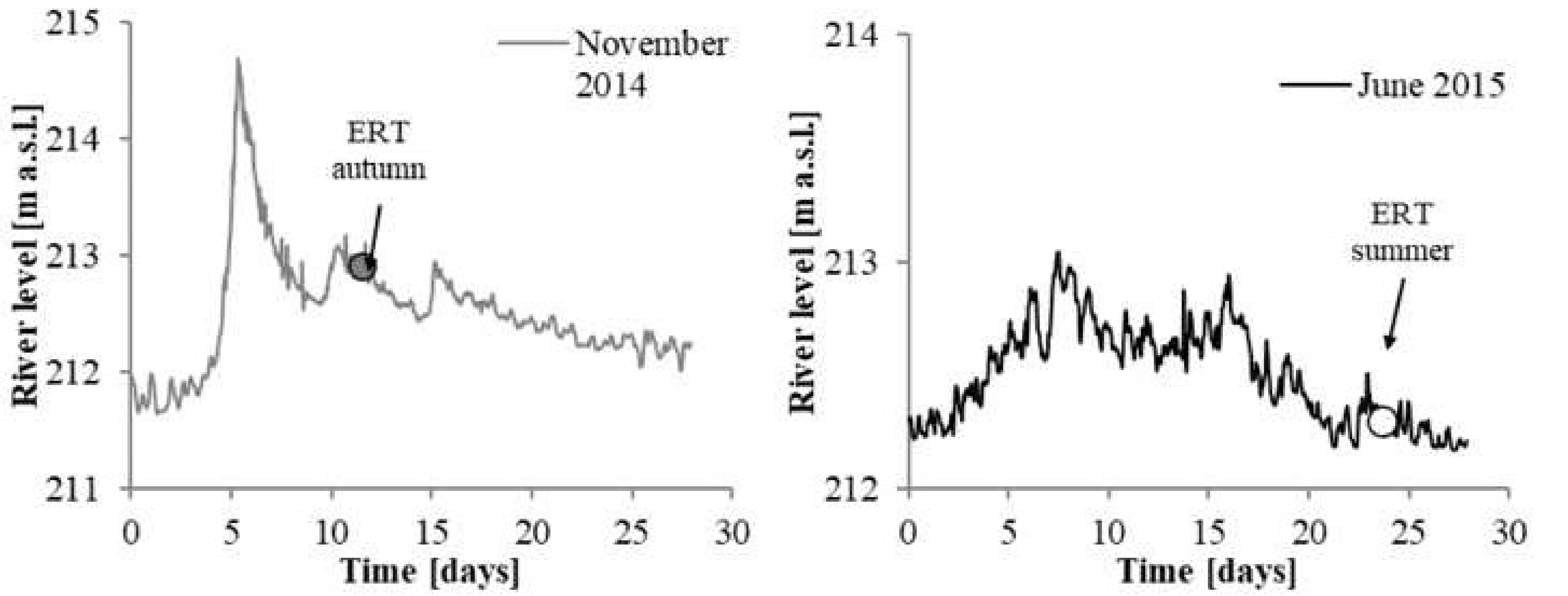
215
214
213
212
211
River level [m a.s.l.]
November 2014
ERT autumn
0
5
10
15
20
25
30
Time [days]
214
213
212
River level [m a.s.l.]
June 2015
ERT summer
0
5
10
15
20
25
30
Time [days]

Figure 13a

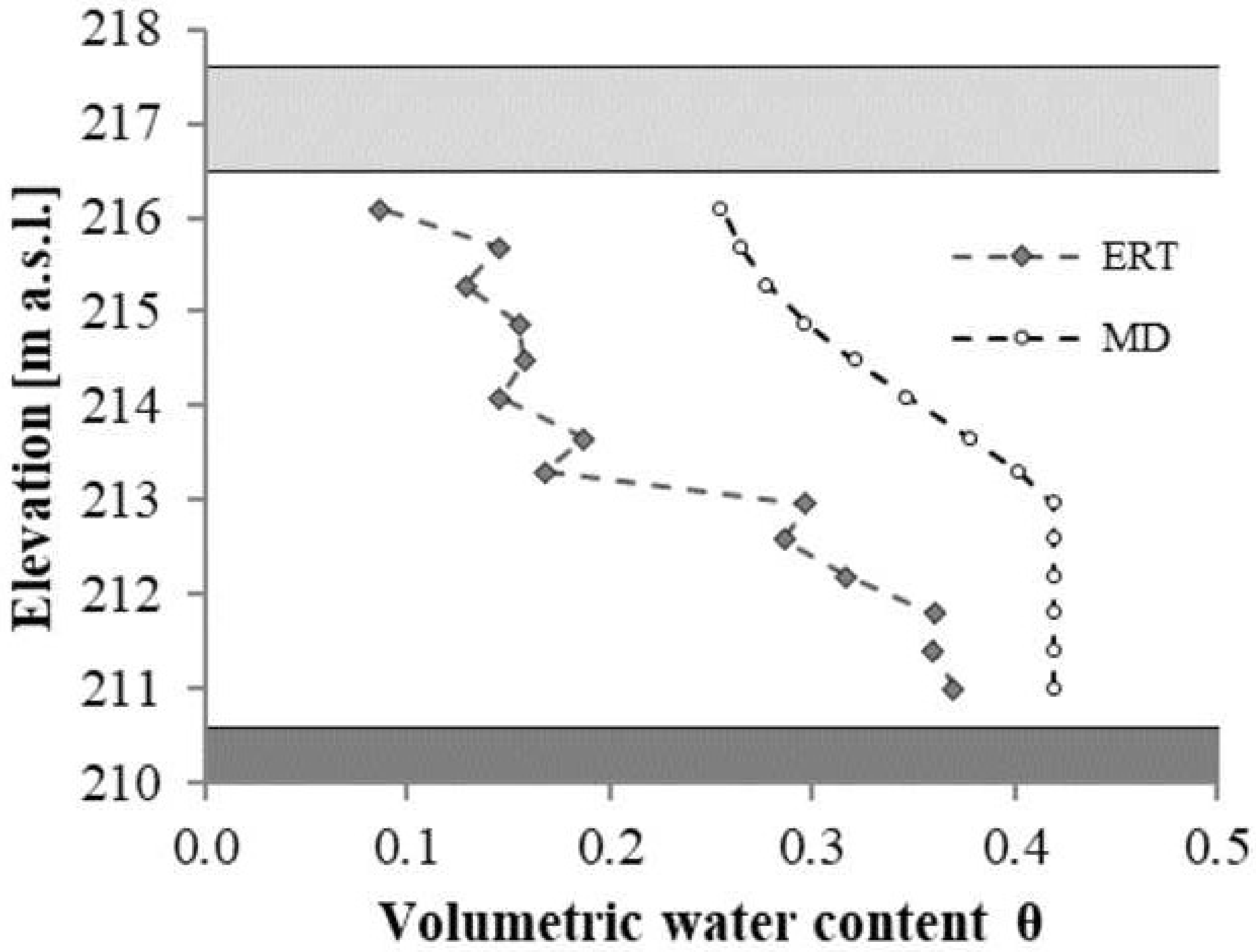
218
217
216
215
214
213
212
211
210
Elevation [m a.s.l.]
0.0
0.1
0.2
0.3
0.4
0.5
Volumetric water content θ
ERT
MD

Figure 13b

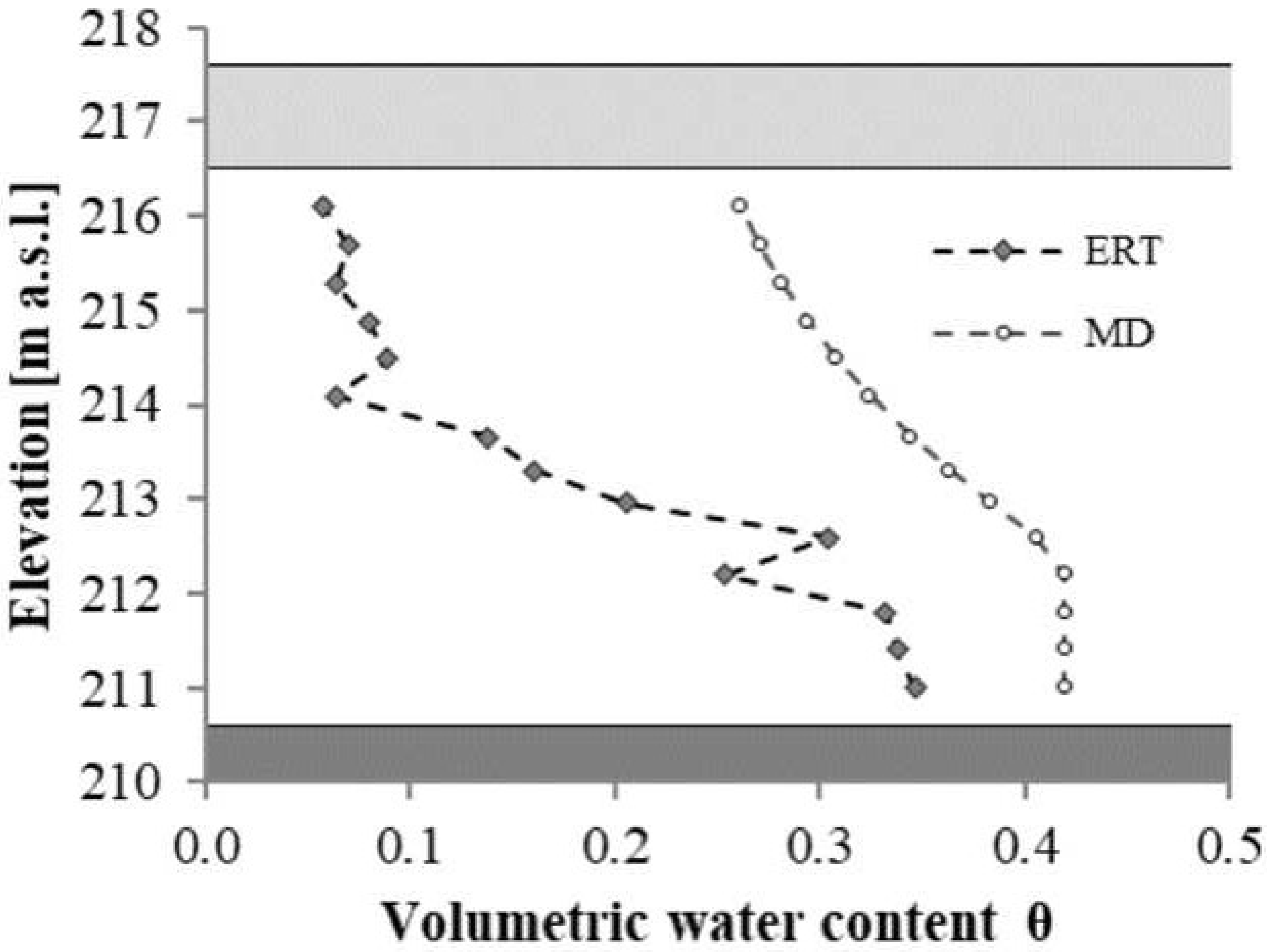
218
217
216
215
214
213
212
211
210
Elevation [m a.s.l.]
0.0
0.1
0.2
0.3
0.4
0.5
Volumetric water content θ
ERT
MD

Figure 14

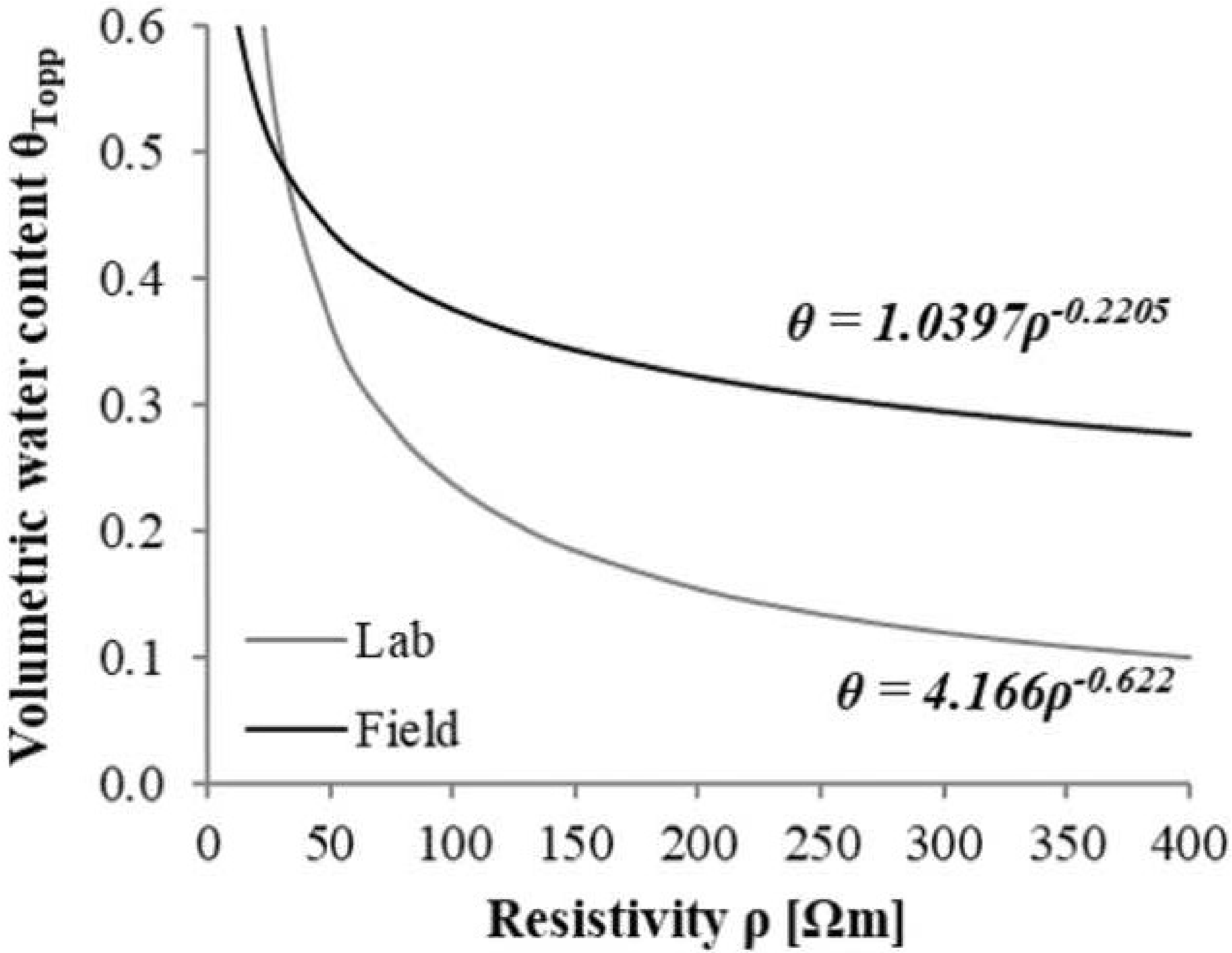

Volumetric water content θ_{Topp}
0.6
0.5
0.4
0.3
0.2
0.1
0.0
0
50
100
150
200
250
300
350
400
Resistivity ρ [Ωm]
Lab
Field
$\theta = 1.0397\rho^{-0.2205}$
$\theta = 4.166\rho^{-0.622}$

Figure 15a

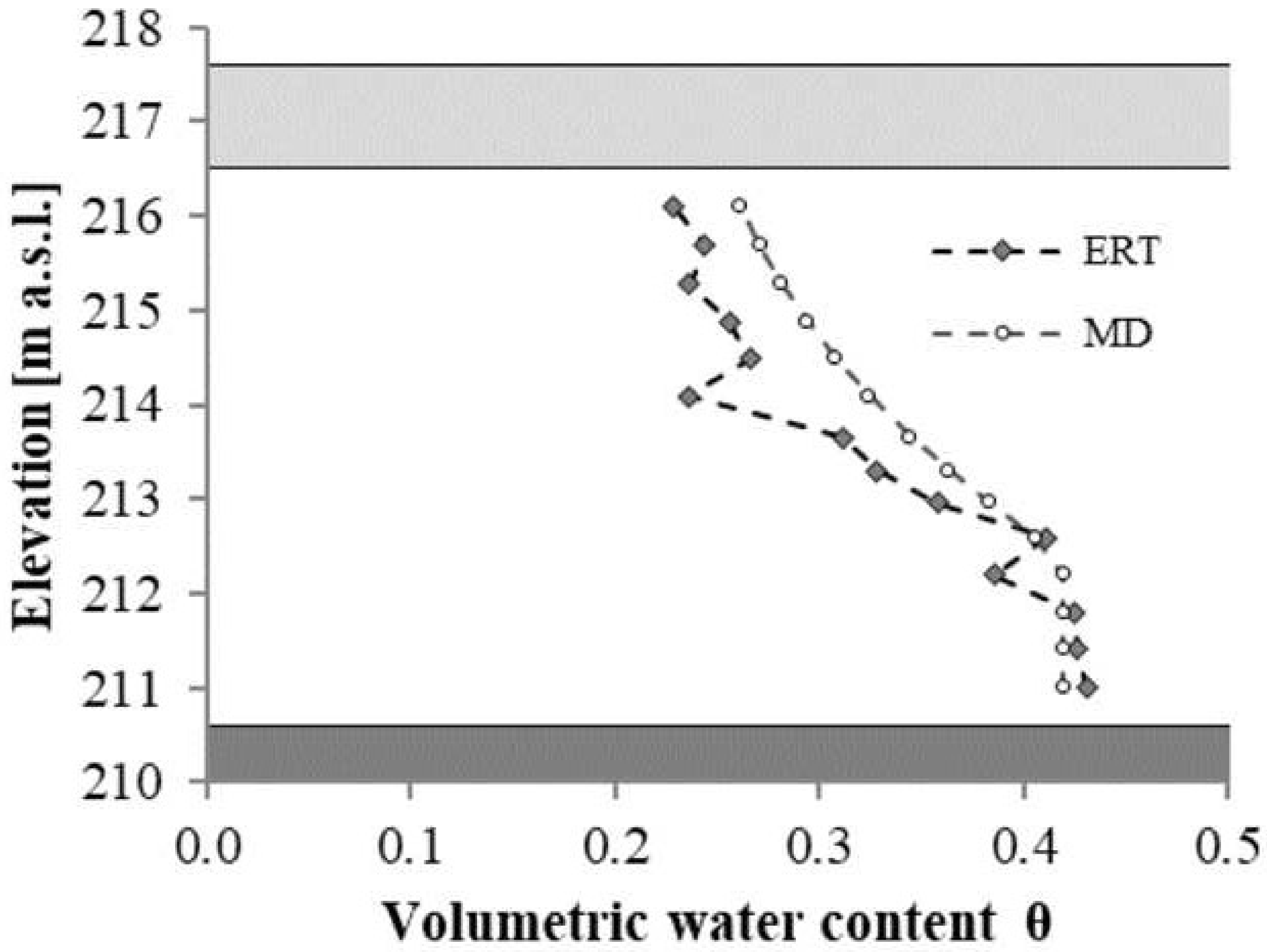
218
217
216
215
214
213
212
211
210
Elevation [m a.s.l.]
0.0
0.1
0.2
0.3
0.4
0.5
Volumetric water content θ
ERT
MD

Figure 15b

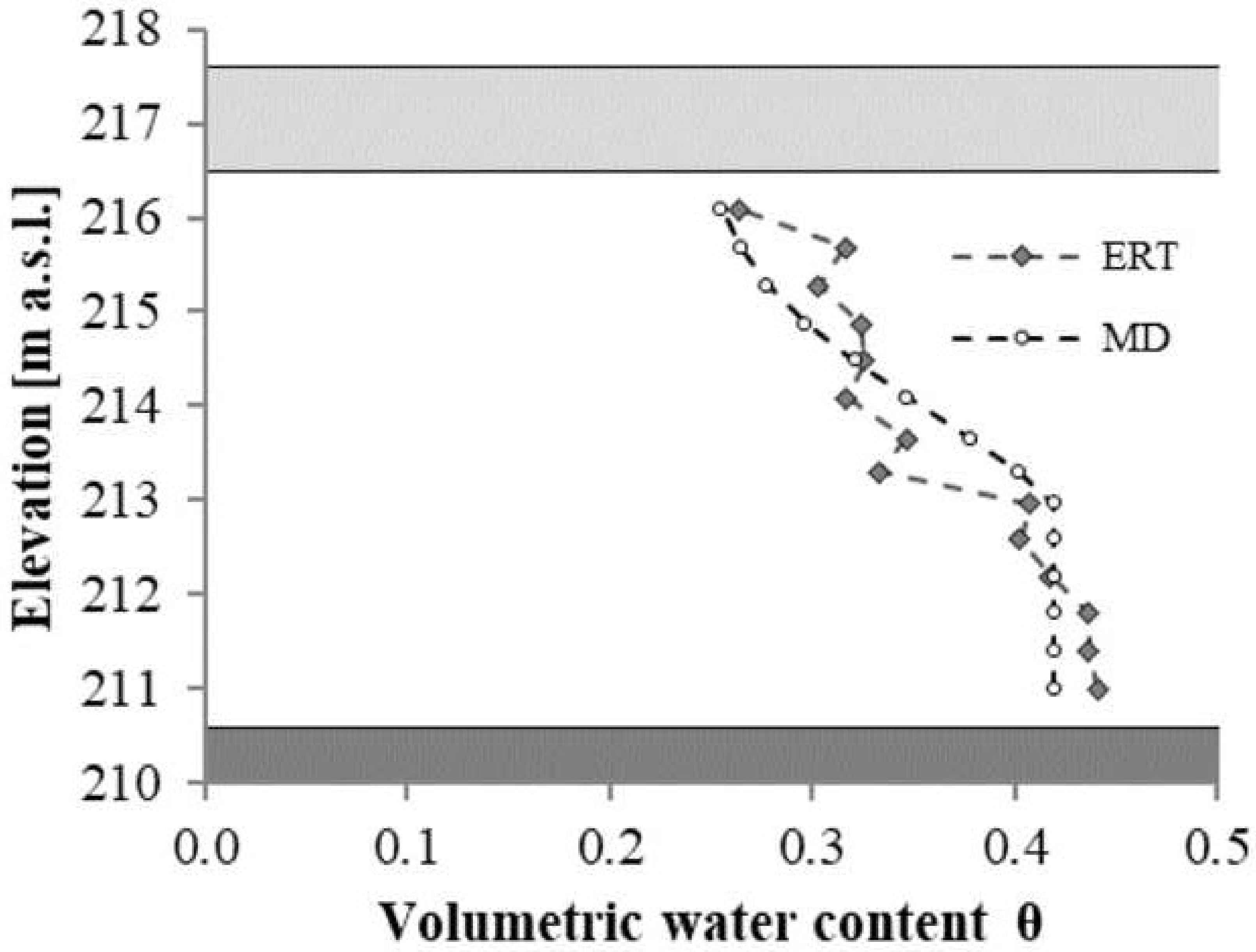
218
217
216
215
214
213
212
211
210
Elevation [m a.s.l.]
0.0
0.1
0.2
0.3
0.4
0.5
Volumetric water content θ
ERT
MD